Warm dense matter studies using ultrafast optical and extreme ultraviolet laser pulses

Ying Y. Tsui
Department of Electrical & Computer Engineering
University of Alberta

Invited Talk presented at the 2020 Annual Congress of the Canadian Association of Physicists

Solid to Plasma Transition
femtosecond optical or XUV laser irradiation

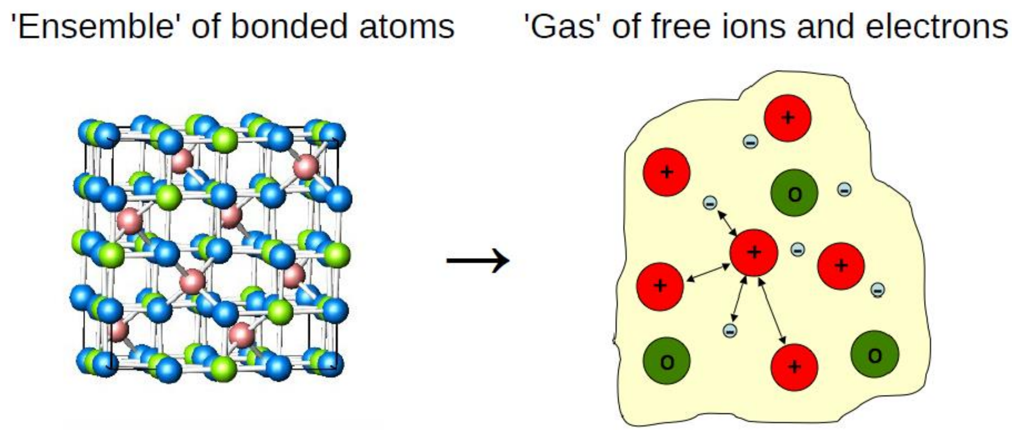

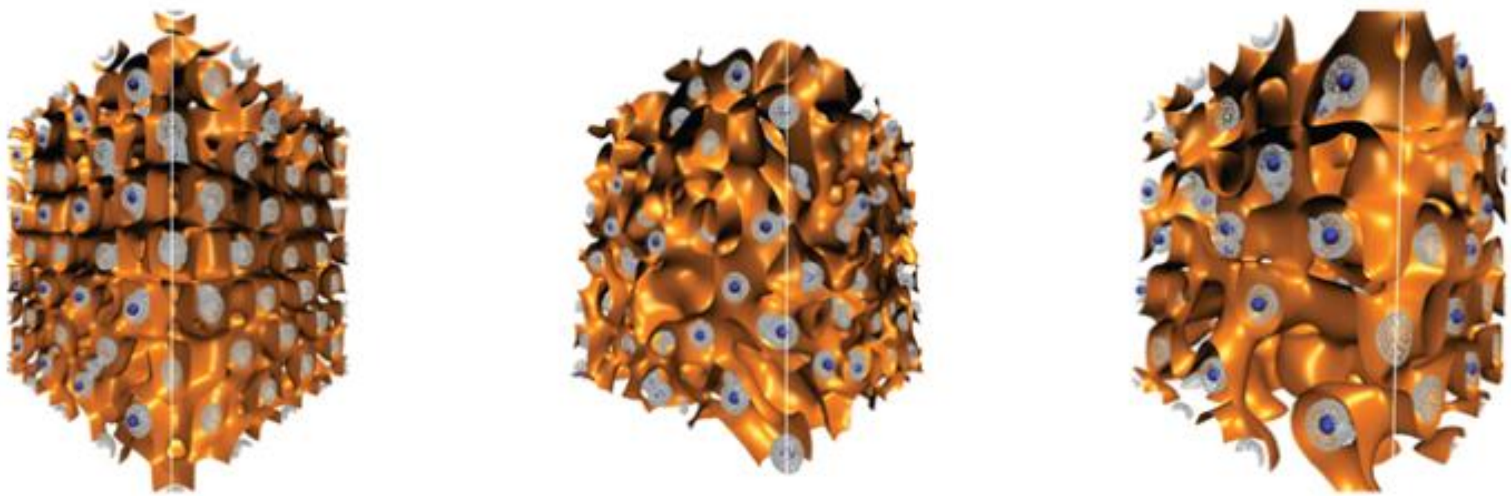

Solid aluminium | Melting phase | Warm dense matter

Molecular dynamics simulations of the formation of WDM indicate that the ions (dark blue) abandon their lattice positions. Although core electrons (grey) remain mostly unchanged, the delocalized conduction electrons (represented by orange isosurfaces) are disturbed from the very regular structure in the lattice. (Credit: SLAC National accelerator Laboratory)

Early time "pre-ablation" physics of ultrafast laser irradiated solids

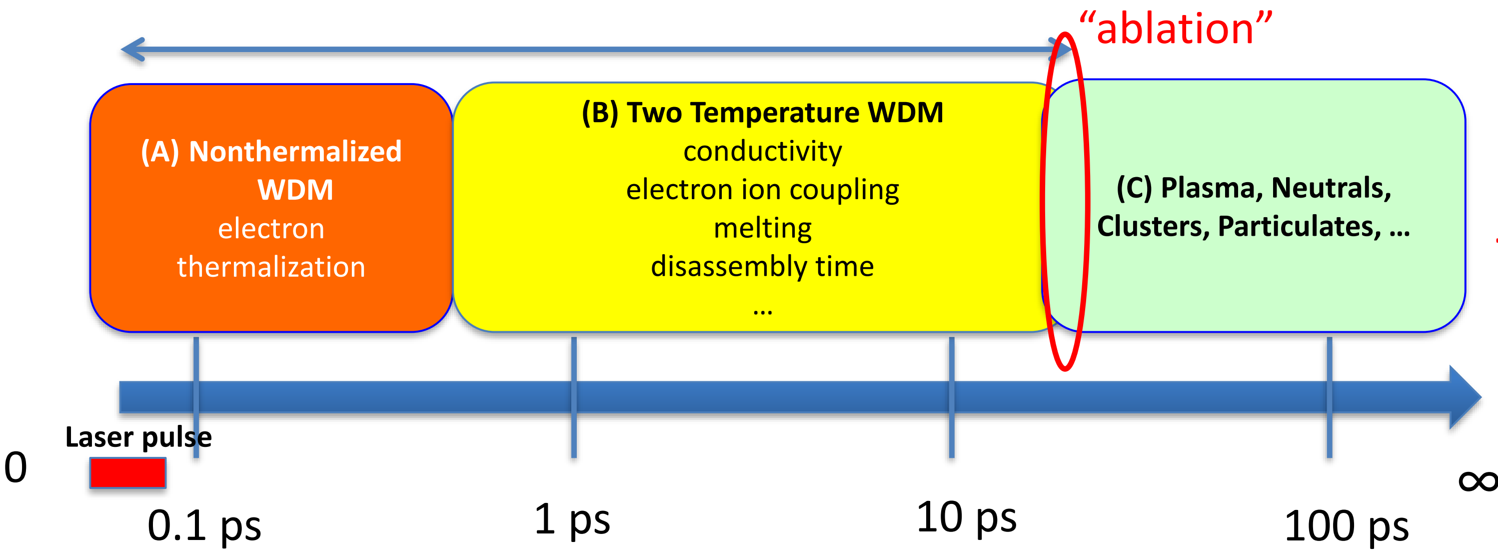

Use ultrafast pump-probe measurements to better understand the first few ps in ultrafast laser matter interaction

(A) Nonthermalized Warm Dense Matter (WDM*)

Chen, (2019 submitted)
- optical R & T probe
- electron kinetics, electron thermalization time

(B) Two Temperature WDM (2T WDM)

Chen, *PRL* (2013)
- optical R & T probe
- AC conductivity, Ce, $\mathbf{g_{ei}}$

Holst, *PRB* (2014)
- DFT-MD & TTM
- AC conductivity, Ce, $\mathbf{g_{ei}}$

Mo, *Science* (2018)
- MeV UED probe
- Melting dynamics, $\mathbf{g_{ei}}$

Chen, *PRL* (2018)
- Optical FDI
- Disassembly time

**WDM – solid density and few eV temperature*

(B) 2T WDM

Chen, *PRL* (2012)
- 2 side optical R probes
- Electron transport

Mo, *PRE* (2016)
- Betatron x-ray
- Ionization dynamics

Ng, *PRE* (2016)
- Modified Drude model
- DC conductivity from AC conductivity

Russell, *OE* (2017)
Chen, (2020 submitted)
- THz probe
- DC conductivity

Two Temperature Model (TTM)

TTM is widely used to model the evolution of T_e, T_i for a laser irradiated solid

$$c_e \frac{\partial T_e}{\partial t} = \frac{\partial}{\partial x}\left(\kappa \frac{\partial T_e}{\partial x}\right) - g_{ei}(T_e - T_i) + A$$

$$c_i \frac{\partial T_i}{\partial t} = g_{ei}(T_e - T_i)$$

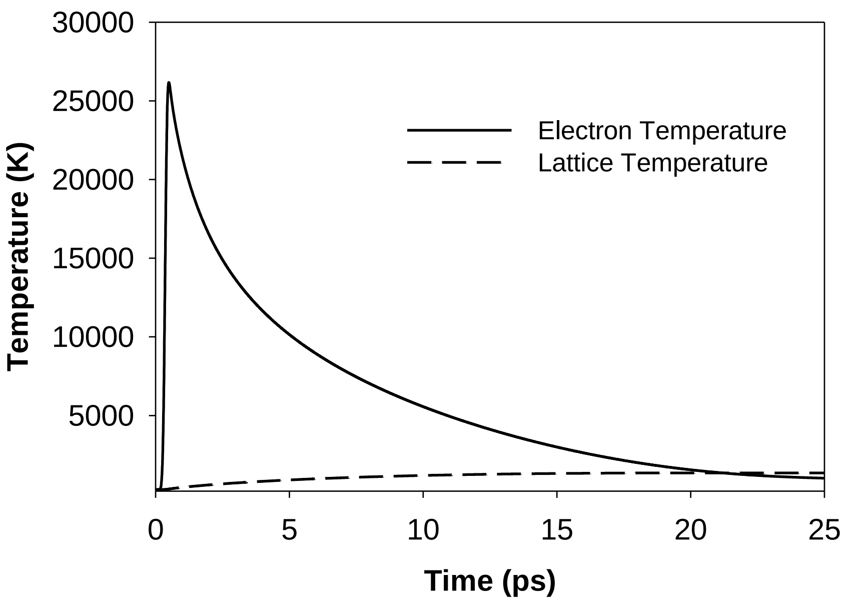

A: absorbed laser power per unit volume

κ: thermal conductivity

C_e : electron heat capacity

g_{ei} : electron ion coupling factor

c_i: ion heat capacity

Electron heat capacity (c_e) of solid gold

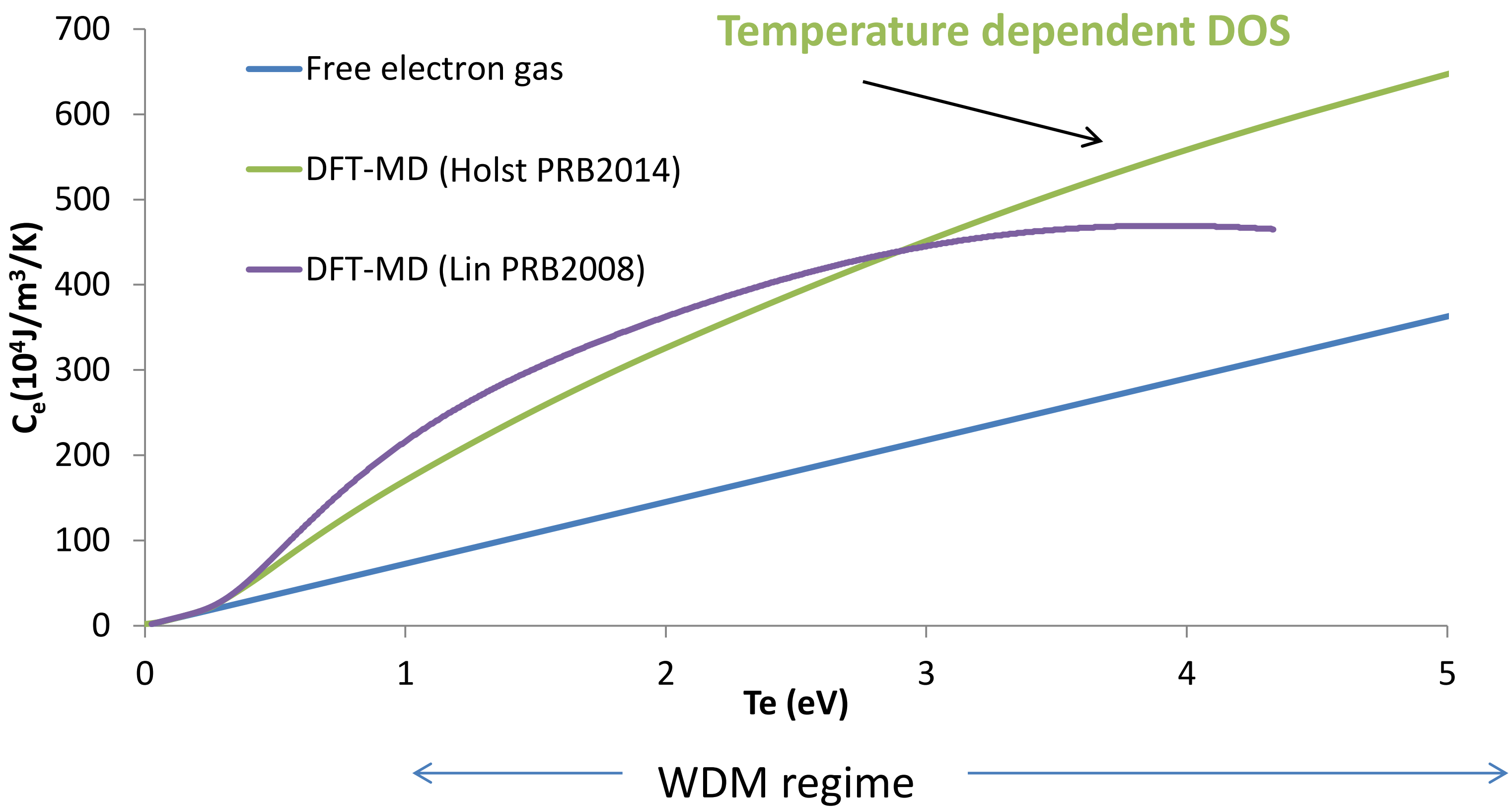

- Agreement found between Density Functional Theory (DFT) calculations
  - Holst, PRB 90, 035121 (2014)
  - Lin, PRB 77, 075133 (2008)
- Need experimental tests

Free electron gas model – Aschrof & Mermin, Solid State Physics

Electron ion coupling factor (g_{ei}) of solid gold

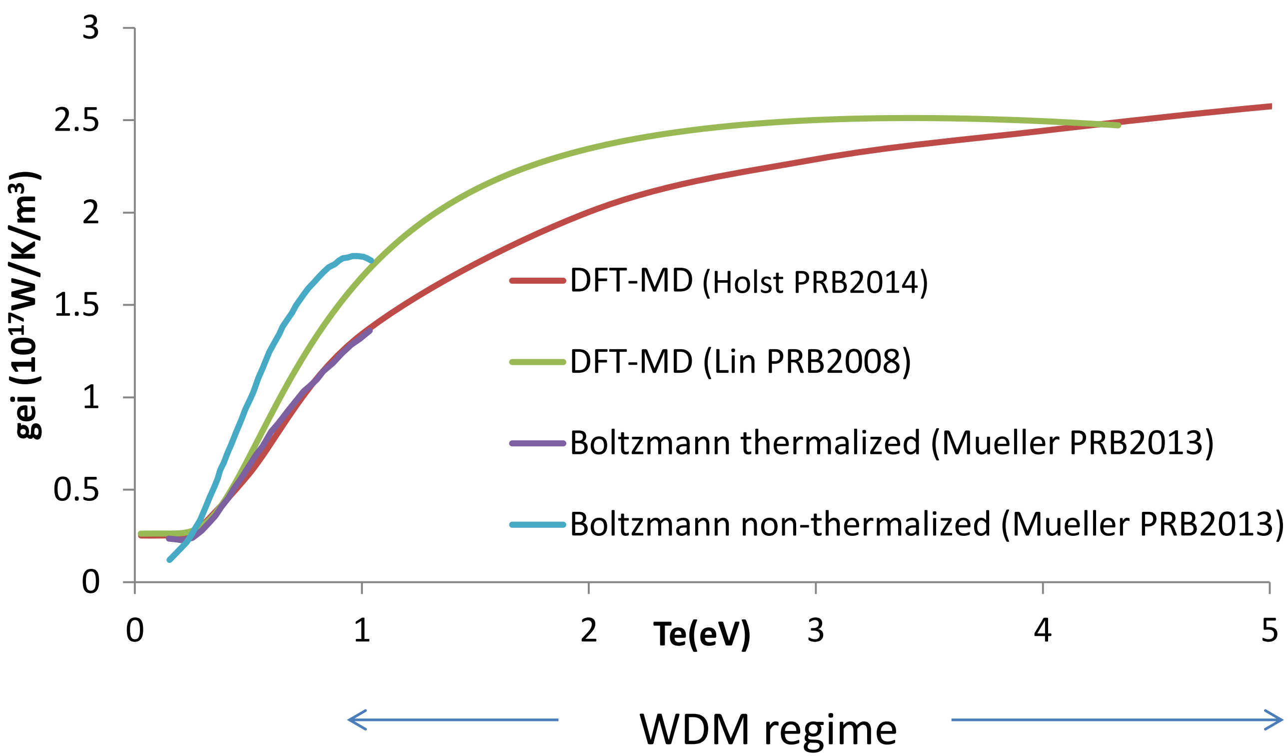

- Reasonable agreement between various theoretical calculations
  - DFT-MD
    [Holst, PRB 90, 035121 (2014)]
    [Lin, PRB 77, 075133 (2008)]
  - Boltzmann Equation with DOS implemented using an one band model
    [Mueller, PRB 87, 035139 (2013)]
- Need experimental tests

Experiment platform for benchmarking calculations

Ultrafast probing of isochoric & uniform heated Au

400nm, 45fs pump laser

Ultrafast Probes

optical (R&T, FDI, 2 side R), MeV UED, THz

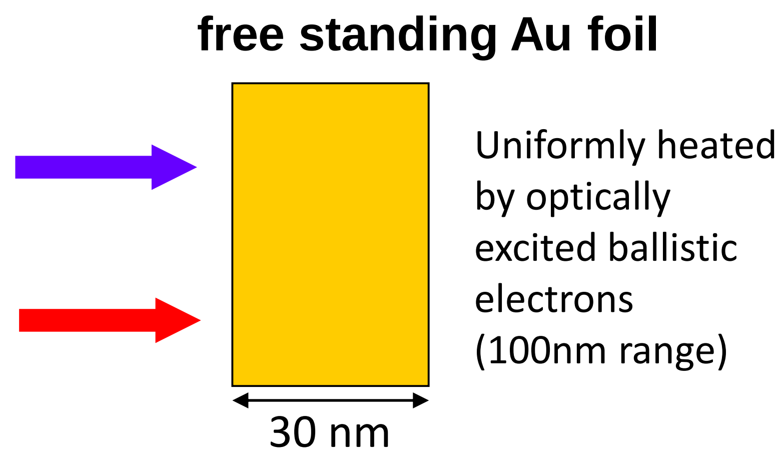

- <u>Isochoric</u> and <u>uniform heated</u> Au
  - 400nm (2ω) ➔ low prepulse; linear absorption by Au
  - Au is chemical inert
  - Gradient free
  - Designed for more direct comparison of experimental results and first principle calculations

Forsman, *PRE* 58, R1248 (1998); Glenzer, *PRL* 90, 175002 (2003); Ng, *Laser & Particle Beams* 23, 527 (2005);

Uniform heated solid gold slab

The evolution of T_e, T_i can be described by the Two Temperature Model

Can be ignored in gradient free system

$$c_e \frac{\partial T_e}{\partial t} = \cancel{\frac{\partial}{\partial x}\left(\kappa \frac{\partial T_e}{\partial x}\right)} - g_{ei}(T_e - T_i) + A$$

$$c_i \frac{\partial T_i}{\partial t} = g_{ei}(T_e - T_i)$$

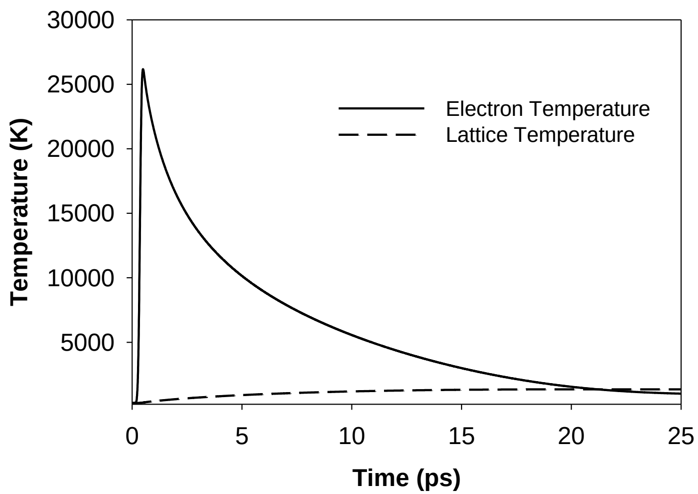

- *A:* absorbed laser power per unit volume
- c_e (T_e): electron heat capacity
- g_{ei} (T_e): electron ion coupling factor
- c_i: ion heat capacity (typically considered to be constant)

AC Conductivity (λ = 800 nm) of ultrafast laser heated gold

- Detailed comparison of experimental and first principle calculated **AC conductivity,** σ_{AC}, at λ = 800 nm, of ultrafast laser heated gold

- Provide experimental tests of first principle calculated $\mathbf{c_e}$ & $\mathbf{g_{ei}}$
  - The initial σ_{AC} value depends on c_e
  - The temporal behaviour of σ_{AC} depends on g_{ei}

Chen, PRL 110, 135001 (2013) & Holst, *PRB* 90, 035121 (2014)

Experimental Setup for Single Shot Reflectivity and Transmissivity Measurement

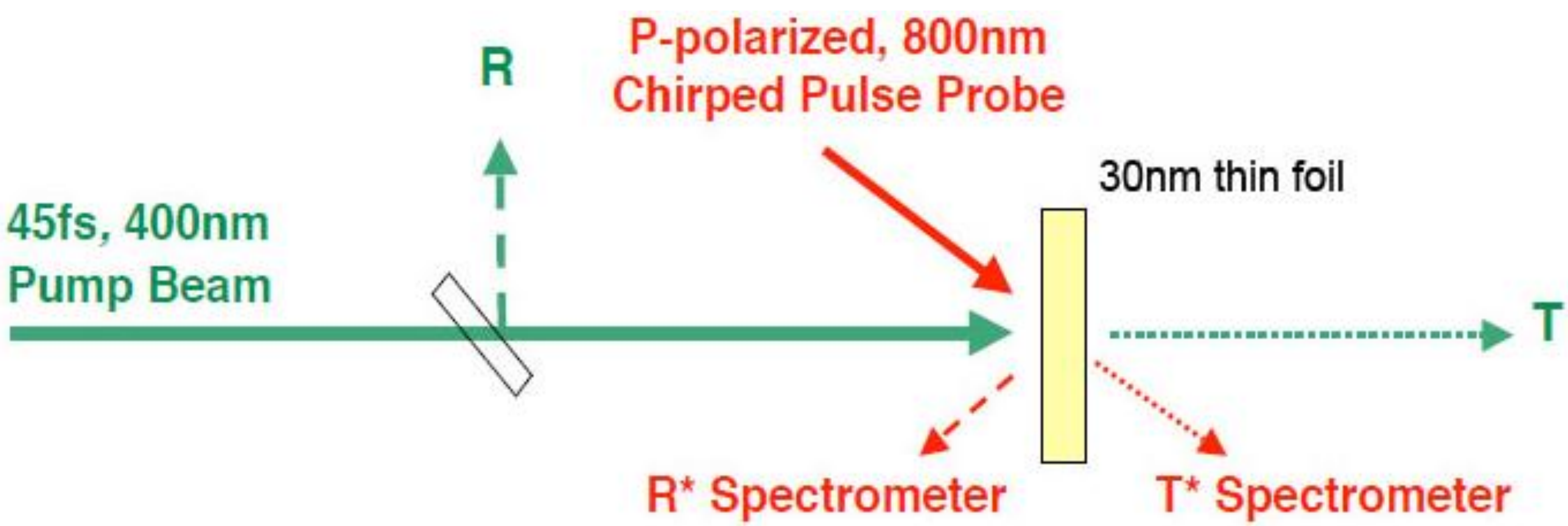

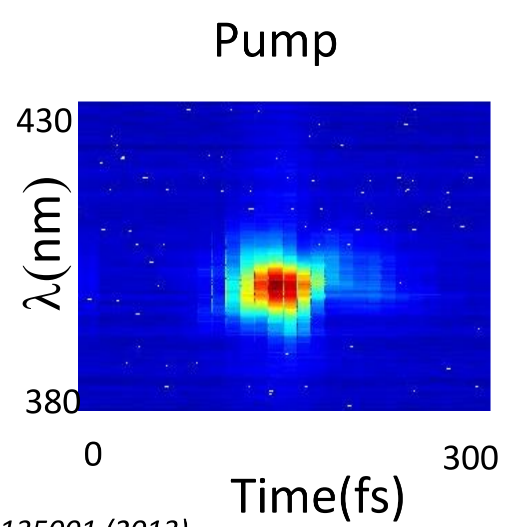

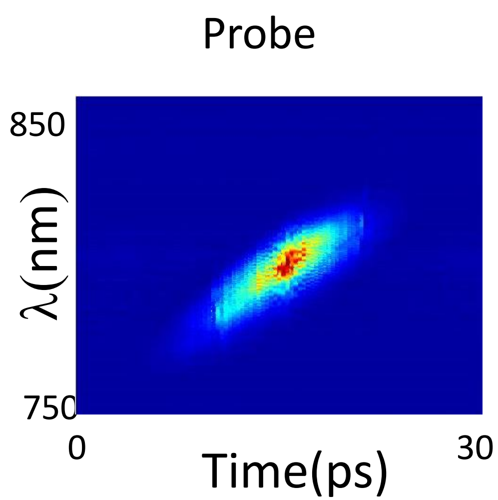

~0.5 ps resolution

Chen, PRL 110, 135001 (2013)

AC conductivity from experimental R &T data

R(t),T(t) -------------------Helmholtz equation solver for a uniform slab-------------------→$\sigma_r(t),\sigma_i(t)$

of Au at λ = 800 nm

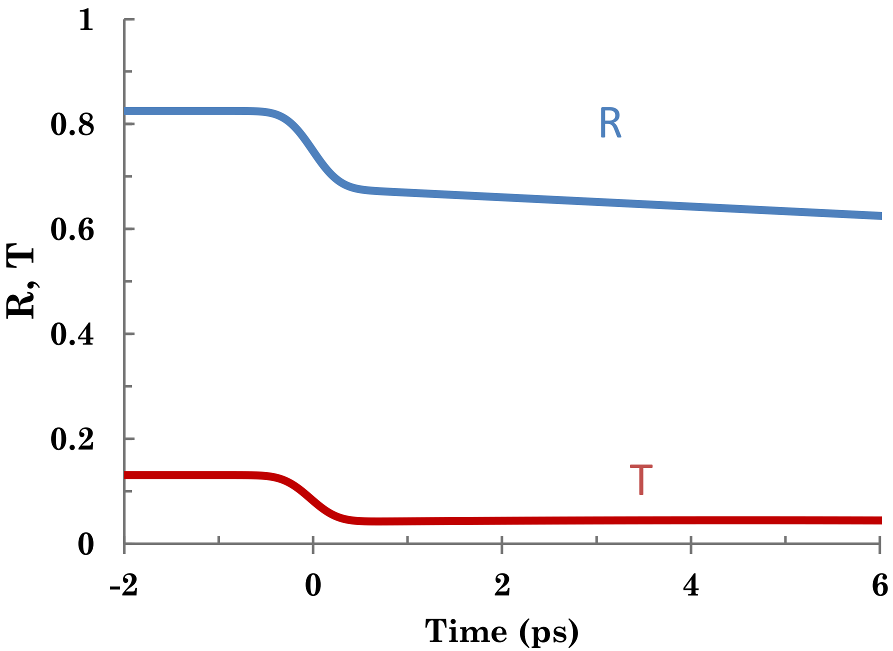

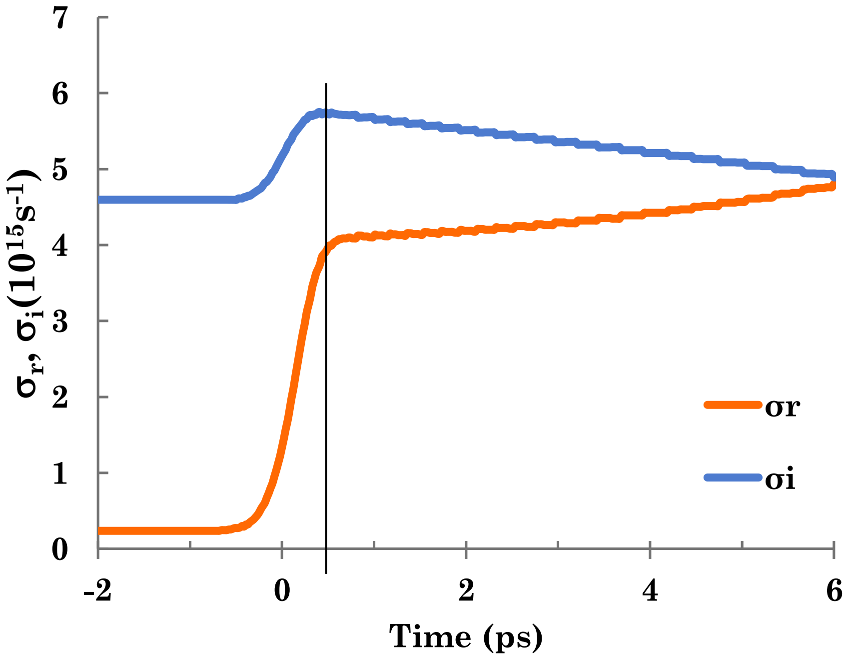

Chen, *PRL* 108, 165001 (2012)

DFT-MD-TTM Calculation of AC Conductivity

- Electron system
  - *ab-initio* plane wave DFT code ABINIT in parallel implementation
- Ion system
  - Molecular Dynamic (MD) simulations
  - Each ionic time step, electronic structure is calculated using DFT
- AC conductivity
  - σ_r calculated from Kubo-Greenwood formula
  - σ_i calculated from Kramers-Kronig relations
- Evolution of T_e and T_i is provided by the TTM
- Electron heat capacity C_e
  - Temperature derivative of electron internal energy at constant volume
- Electron-ion coupling factor g_{ei}
  - Similar to [Lin et al, PRB 77, 075133 (2008)]
  - Treating the electron-ion heat transfer rate with electron-phonon scattering in terms of electron and phonon occupation number

Holst, *PRB* 90, 035121 (2014)

Optical R&T Result #1

AC conductivity σ(t ~ 0.5ps) after electrons are thermalized led to information on electron capacity (C_e)

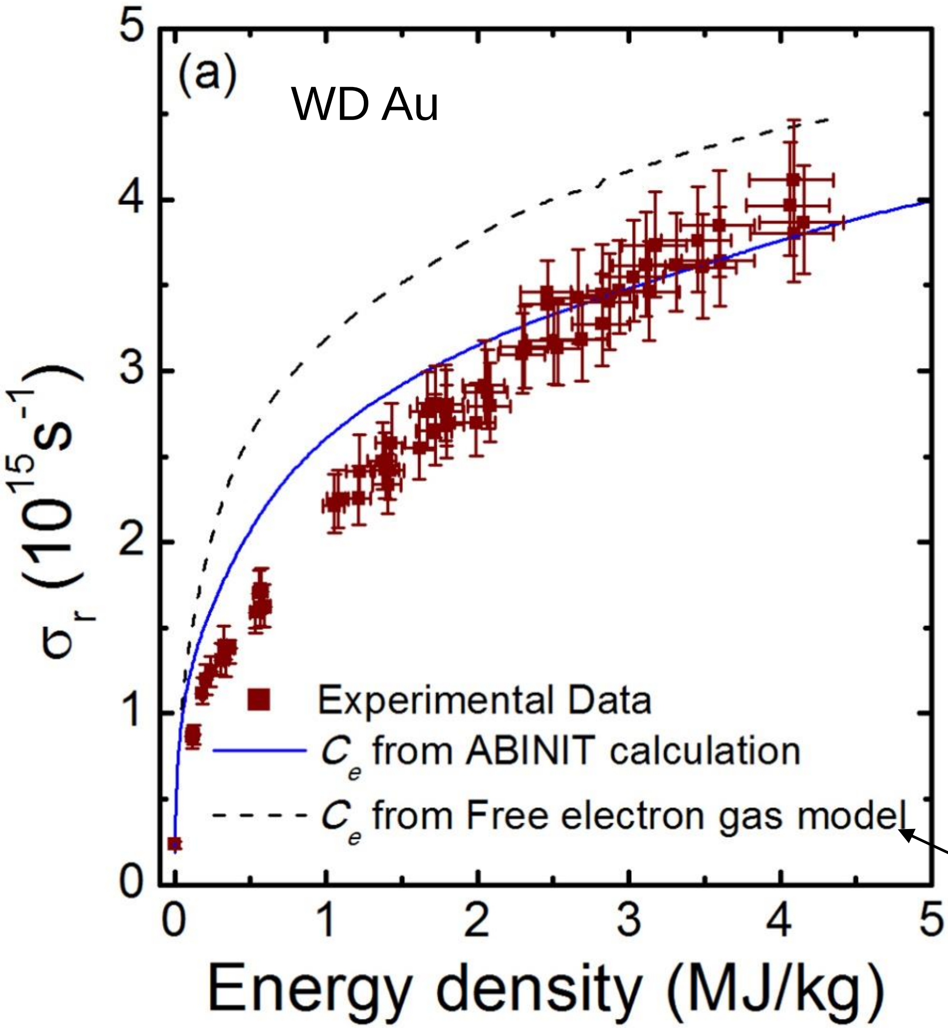

- AC conductivity (λ=800nm) deduced from R & T measurement
- Reasonable agreement was found between experimental and DFT-MD calculated values for σ_r (t ~ 0.5ps) when DFT calculated C_e was used
- **DFT calculated C_e is consistent with experimental result!**

from graduate level textbook

1 MJ/kg ↔ F_{ab} = 63 mJ/cm^2

Chen, PRL 110, 135001 (2013); Holst, PRB 90, 035121 (2014)

1 MJ/kg ↔
F_{ab} = 63 mJ/cm²

Optical R&T Result #2

Temporal evolution of AC conductivity σ(t) led to information on electron-ion coupling (g_{ei})

- Discrepancies between experimental (lines) and calculated (symbol "**o**" using DFT calculated g_{ei}) σ(t)
- A constant g_{ei} would give better agreement i.e. g_{ei} has weak T_e dependence

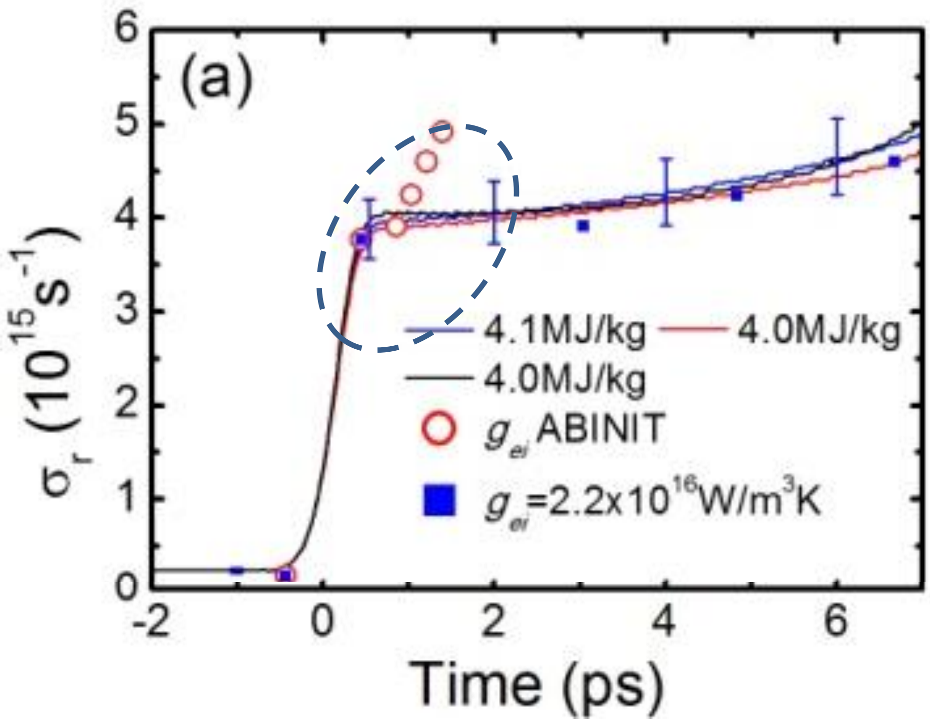

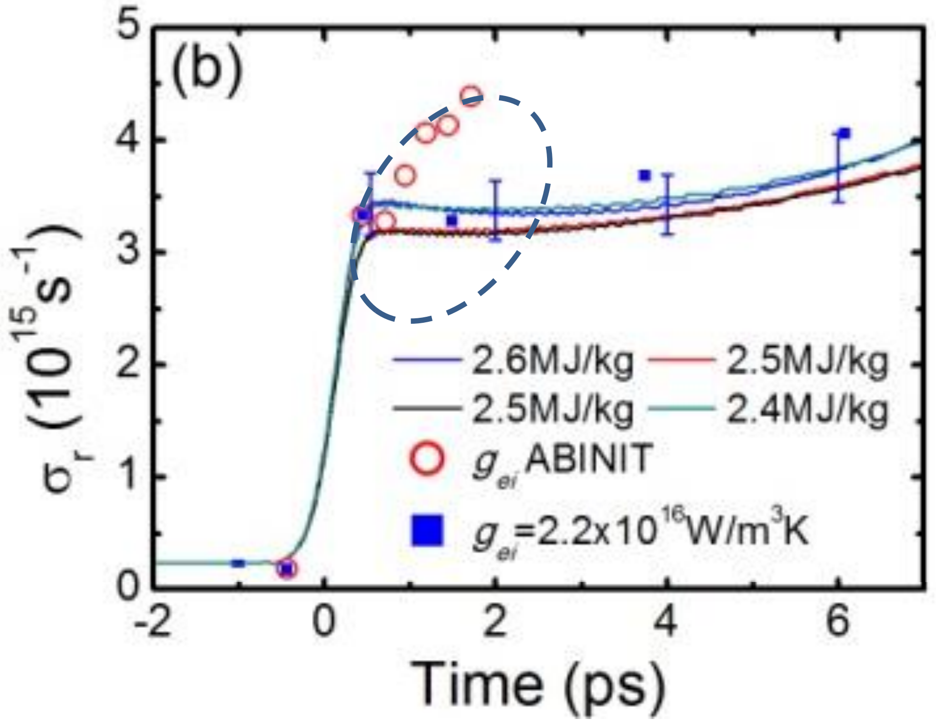

Calculated g_{ei} is not consistent with experimental results

Chen, PRL 110, 135001 (2013); Holst, PRB 90, 035121 (2014)

MeV-UED has been used to study structural dynamics of warm dense gold

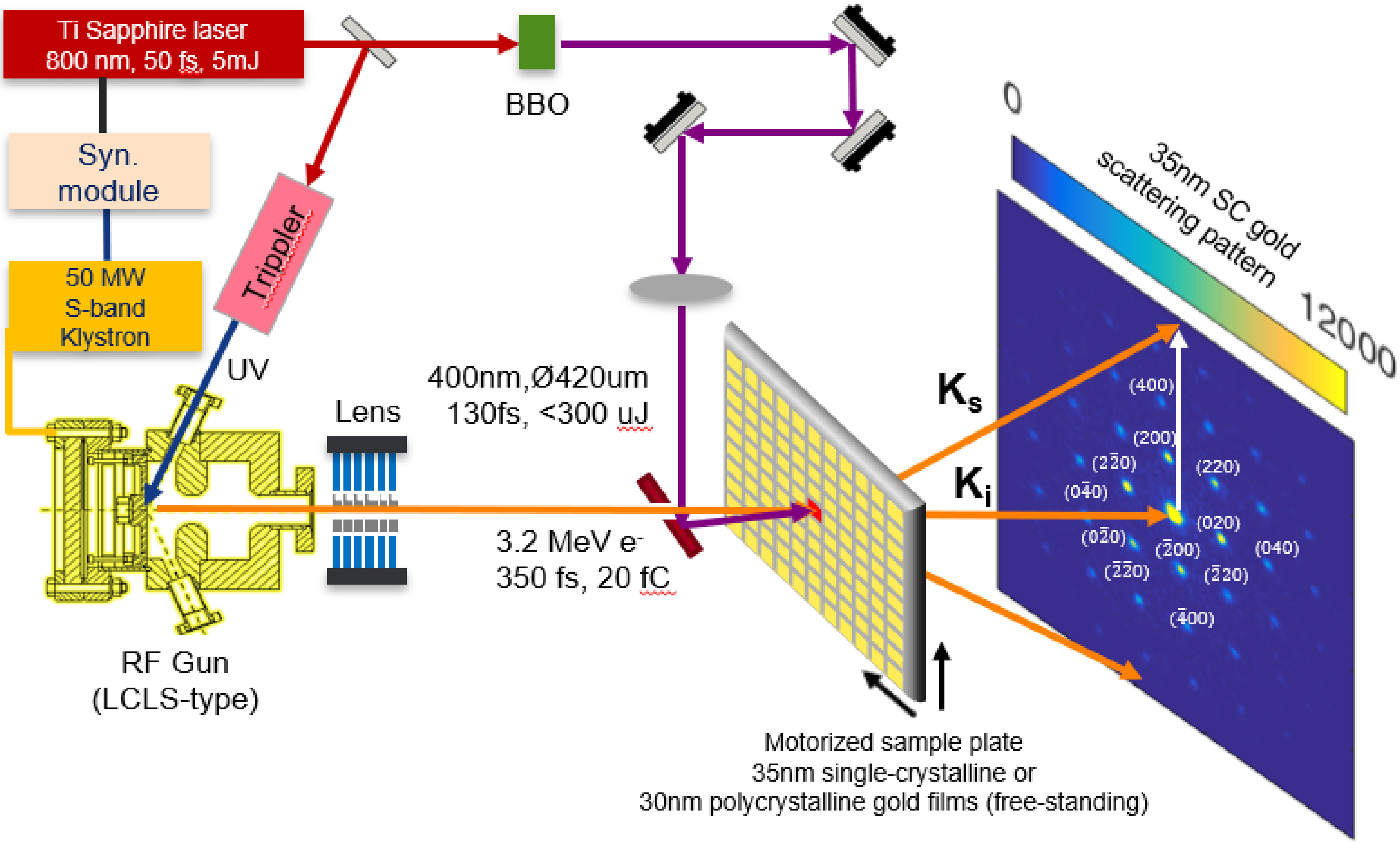

Mo, *RSI* 87, 11D810 (2016)

Optical Pump – Ultrafast Electron (UED) Probe

Key Results: #1 - first time observation of heterogeneous melting
#2 - electron phonon coupling factor - g_{ei}, ~ constant

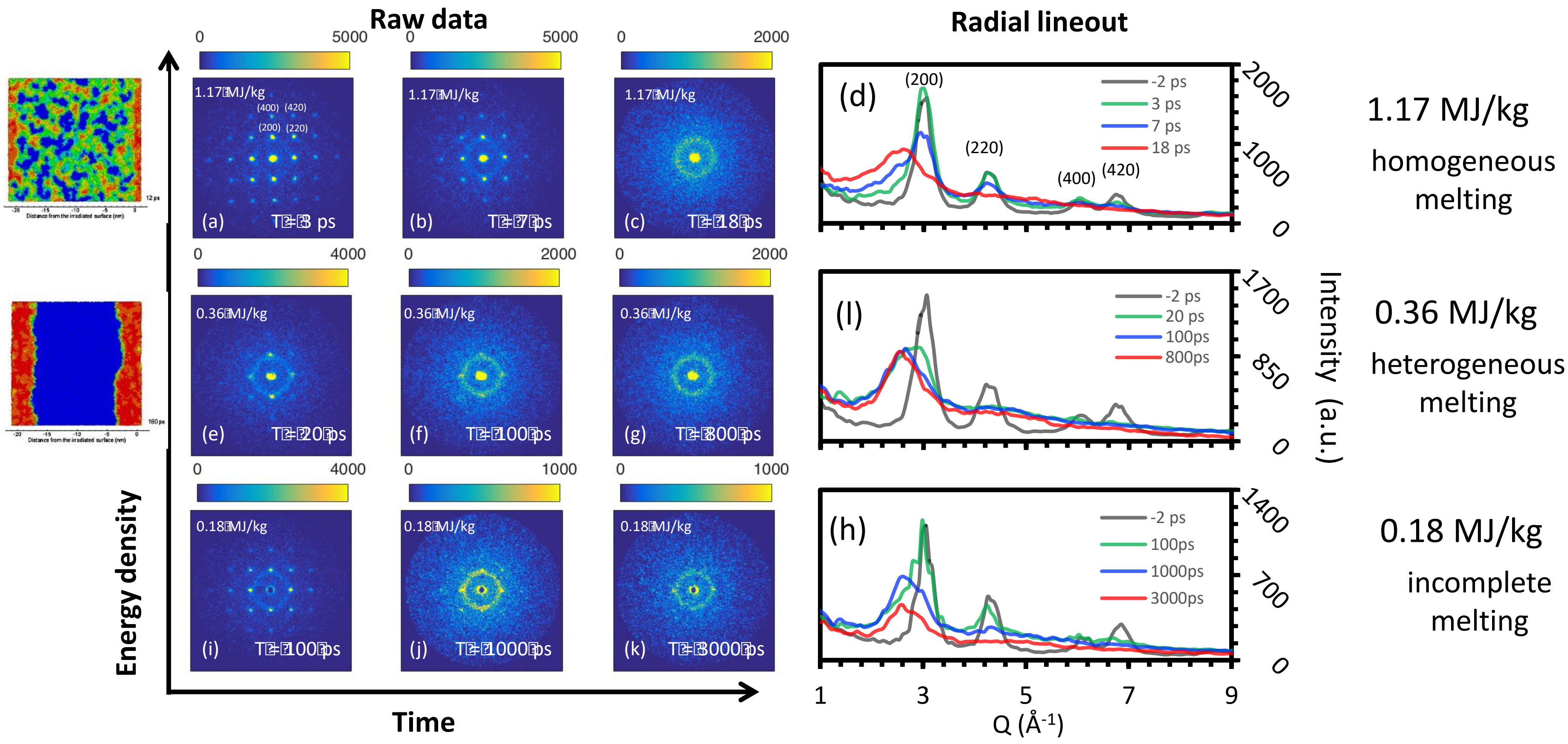

Mo et al, Science 360, 1451 (2018)

Optical Pump – Ultrafast Electron (UED) Probe

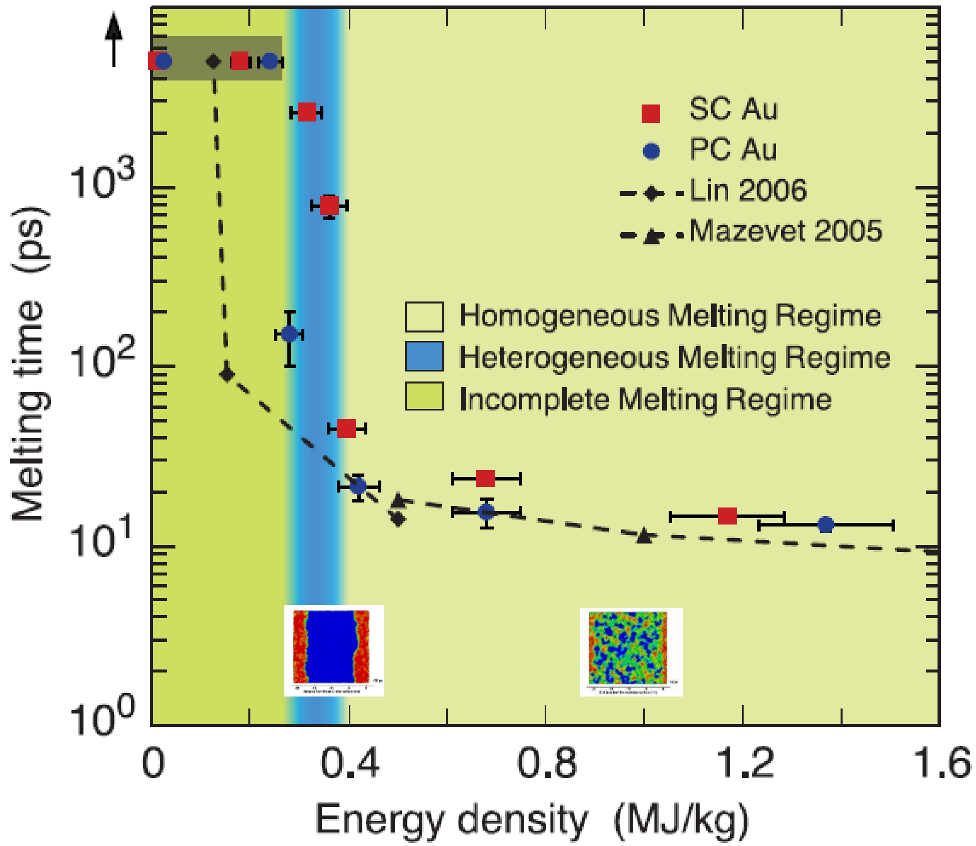

Fig. 3. Energy density dependence of ultrafast laser–induced melting mechanisms in gold. The measured melting time of SC gold and PC gold are represented by red squares and blue circles, respectively, as compared with TTM-MD simulation by Lin *et al.* (*9*) and Mazevet *et al.* (*13*). The vertical error bars are given by the time step intervals around the observed melting times, whereas the horizontal error bars represent 1 SD uncertainty of the measured absorbed energy density. Three melting regimes—homogeneous, heterogeneous, and incomplete melting—are identified from the measurements and indicated by the various background colors. The data located inside the gray shaded area are beyond the instrument limit of 3 ns for our experiments, and the two data points on the left are from measurements of below damage threshold.

Mo et al, Science 360, 1451 (2018)

Ultrafast Electron Diffraction (UED) Result

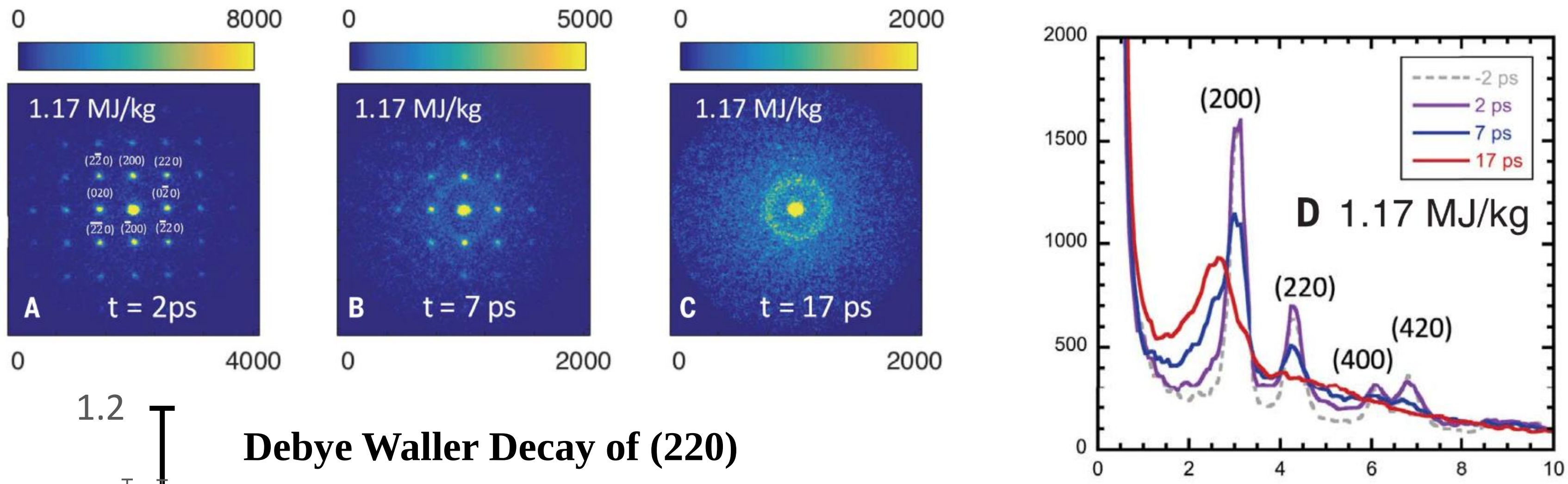

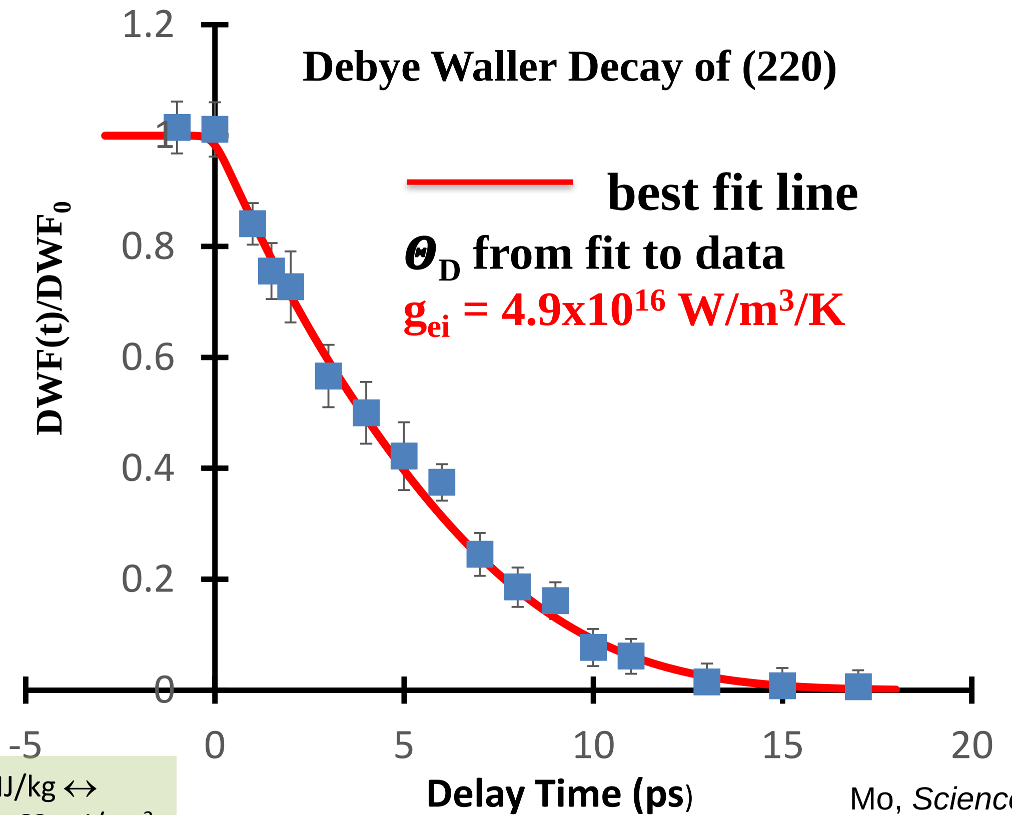

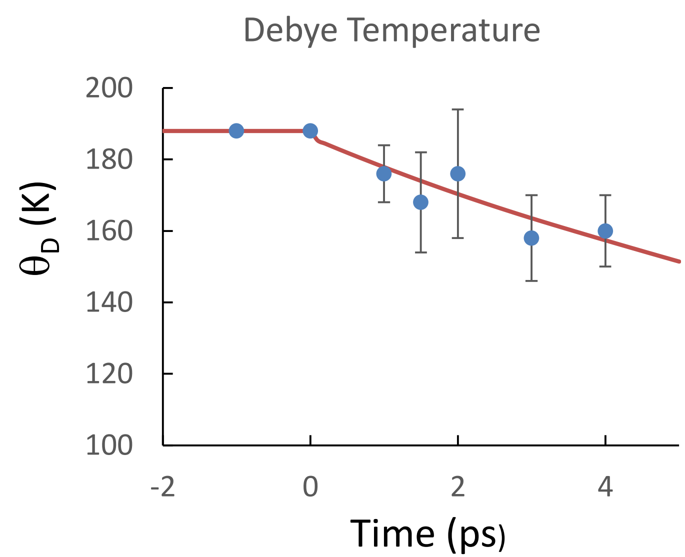

1 MJ/kg ↔
F_{ab} = 63 mJ/cm^2

Mo, *Science* 360, 1451 (2018)

Frequency Domain Interferometry Measurement

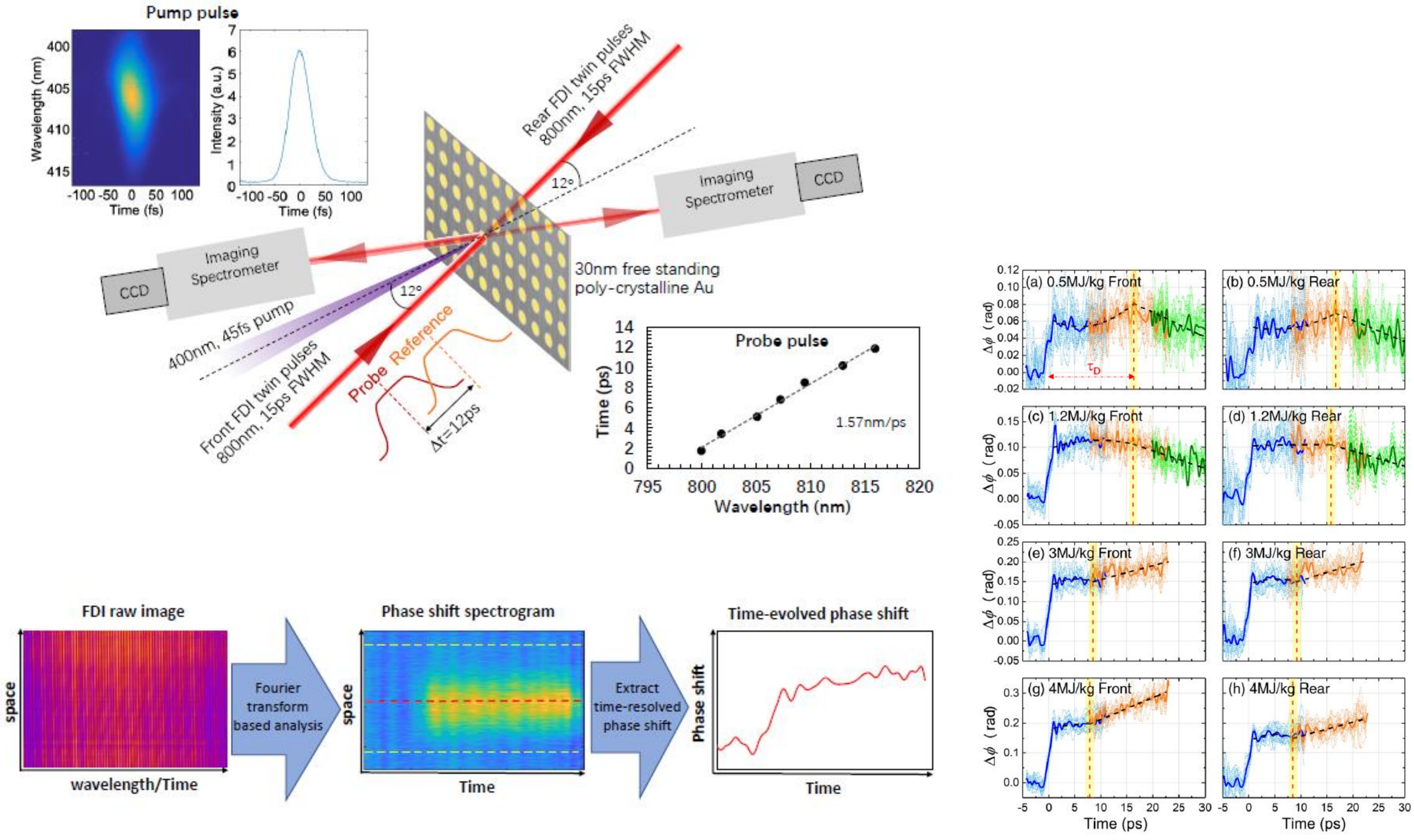

Chen et al, PRL 121, 075002 (2018)

Disassembly Time

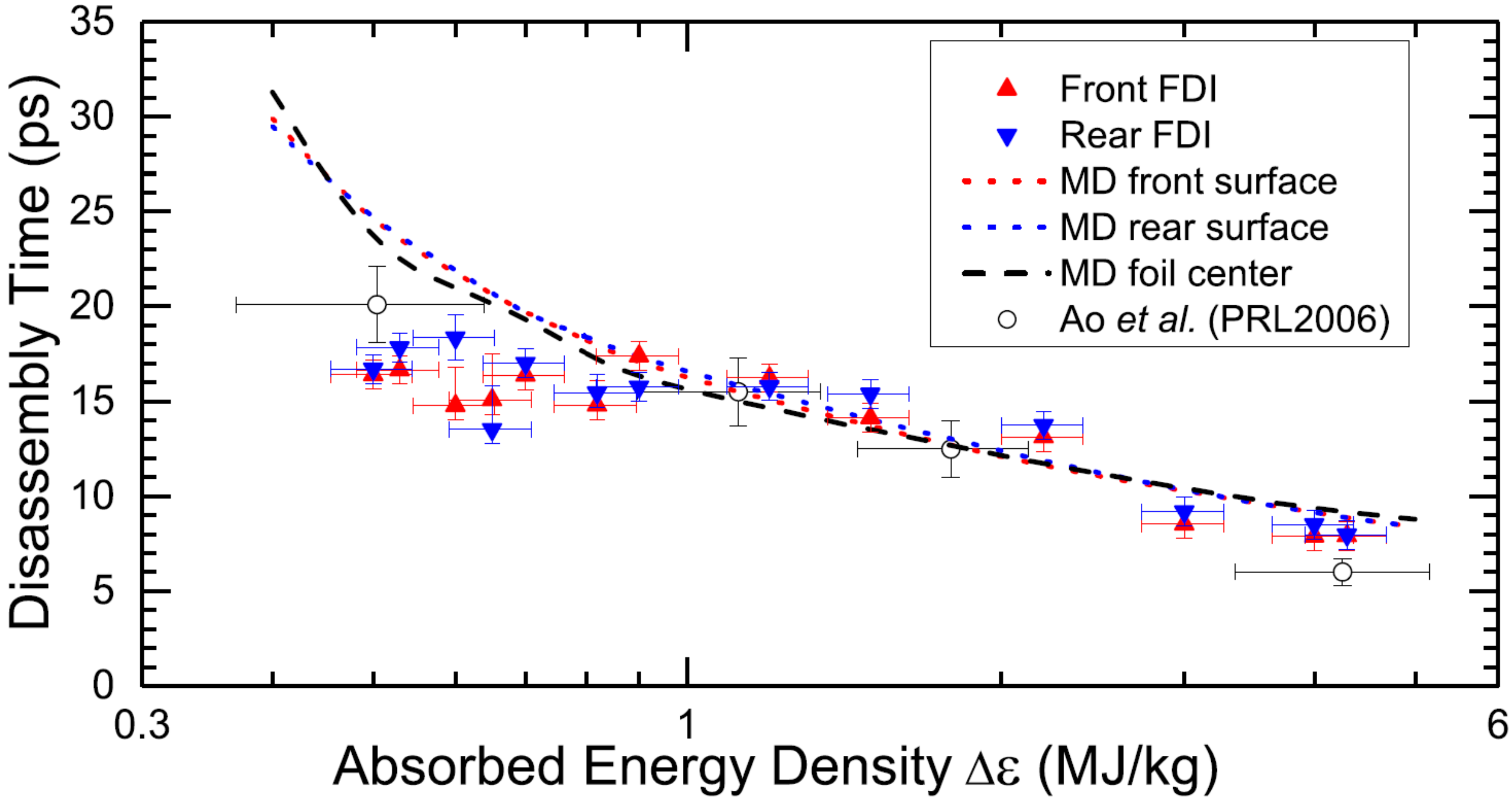

Chen et al, PRL 121, 075002 (2018)

2T-MD used a highly optimized embedded-atom-method interatomic potential and g_{ei} = 2.1×10^{16} W/m^3/K

FDI Disassembly Time & UED Melt Time

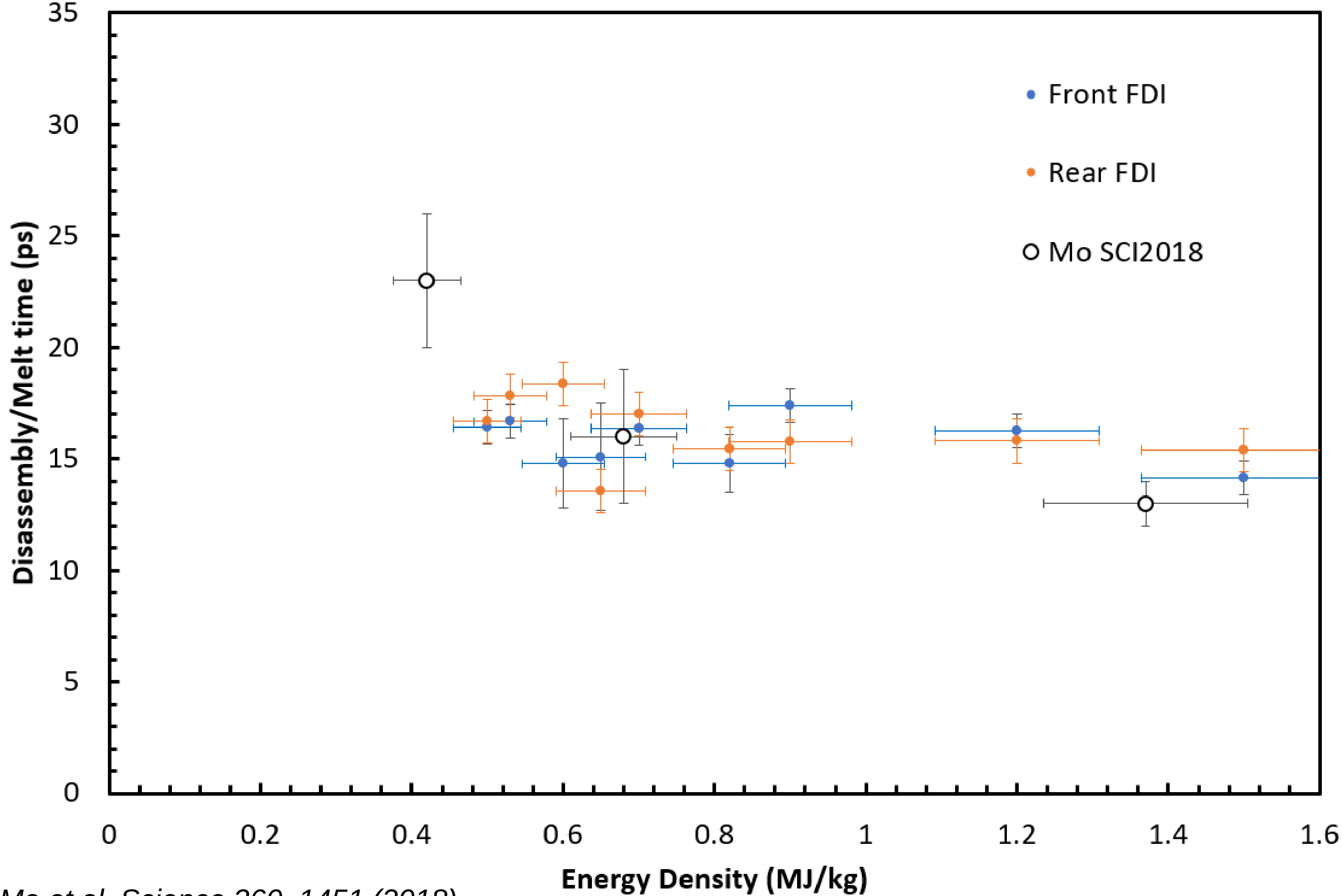

Mo et al, Science 360, 1451 (2018)
Chen et al, PRL 121, 075002 (2018)

Optical R&T, UED and THz measurements

AC conductivity and UED data are robust

I. Our single-shot AC conductivity data is consistent with previous multi-shot data [1]

II. Our AC conductivity data was used to extract DC conductivity based on a modified Drude model [2] and the extracted DC conductivity is consistent with DC conductivity measured directly using a THz probe [3]

III. Our MeV UED data is consistent with previous keV UED data [4]

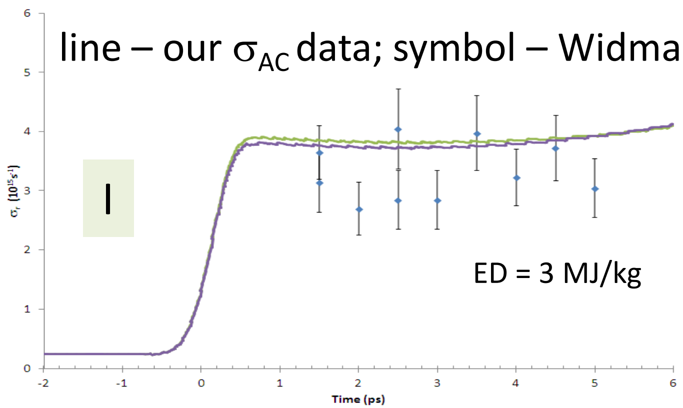

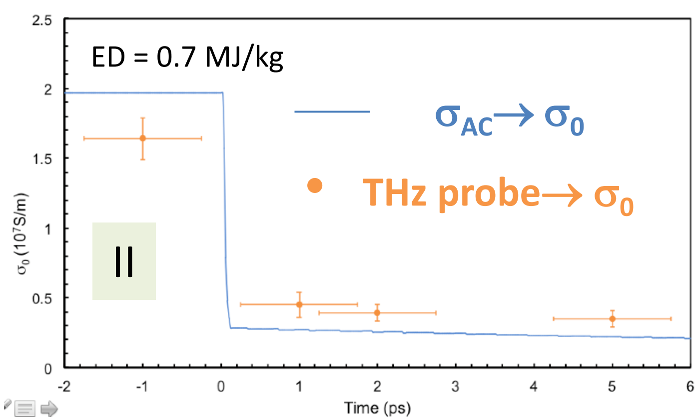

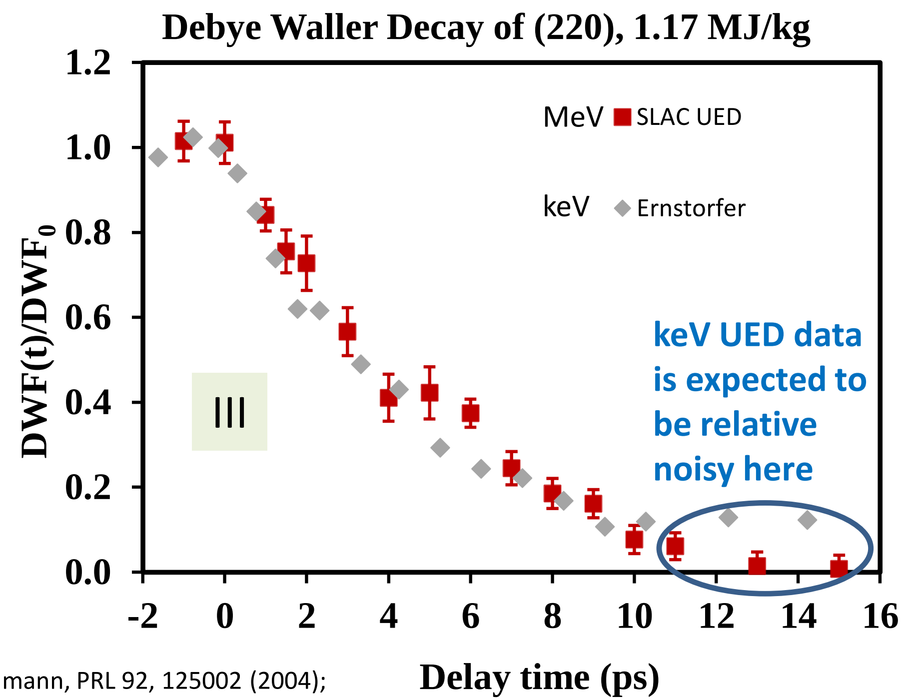

[1] Widmann, PRL 92, 125002 (2004);
[2] Ng, PRE 94, 033213 (2016);
[3] Chen (to be published);
[4] Ernstorfer, Science 323, 1033 (2009)

Theoretical Approaches

- Single electron-phonon scattering picture used in the traditional DFT calculations of g_{ei} may be insufficient.
- Dharma-wardana & Perrot's work suggested that electron and ion density fluctuations in warm dense matter may need to treat as coupled mode. This leads to significantly weaker electron ion coupling.
  - M.W. C. Dharma-wardana and F. Perrot, Phys. Rev. E 58, 3705 (1998).
- Vorberger et al's work reported similar finding.
  - J. Vorberger, D. O. Gericke, T. Bornath, and M. Schlanges, Phys. Rev. E 81, 046404 (2010).
- Medvedev & Milov's most recent calculations predicted weak electron ion coupling for gold. They used an dynamical coupling approach to calculate the nonadiabatic electron-ion energy exchange in nonequilibrium solids with high electronic temperature
  - N. Medvedev & I. Milov, "Electron-phonon coupling in metals at high electronic temperatures", arXiv:2005.05186 (posted May 11, 2020)
  - N. Medvedev, Z. Li, V. Tkachenko & B. Ziajia, Phys. Rev. B95, 014309 (2017).

Free-Electron-Lasers (FELs)
4th Generation Light Source

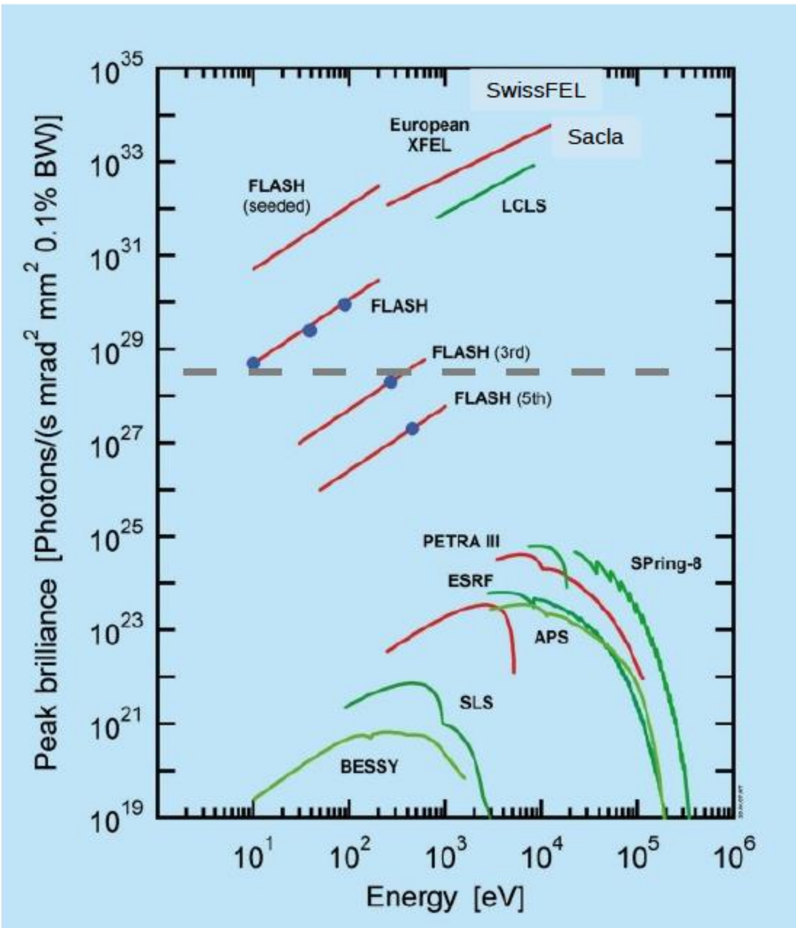

photon-science.desy.de

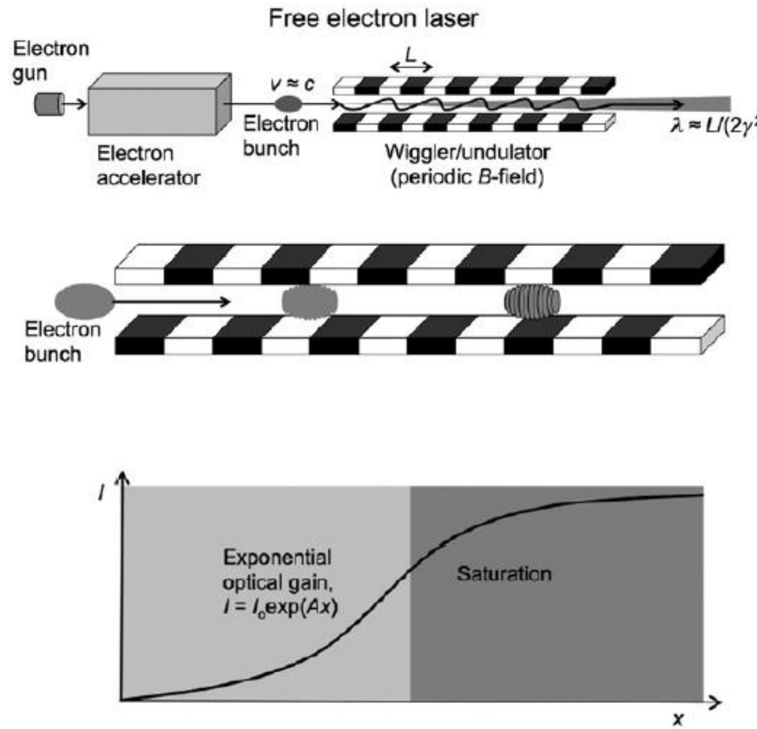

Ribic, Margaritondo, J. Phys. D **45** 213001 (2012)

Pulse duration ~ down to 10 fs
Wavelength ~ VUV- hard X-ray

XUV Generated Warm Dense Gold

FLASH Experimental Setup

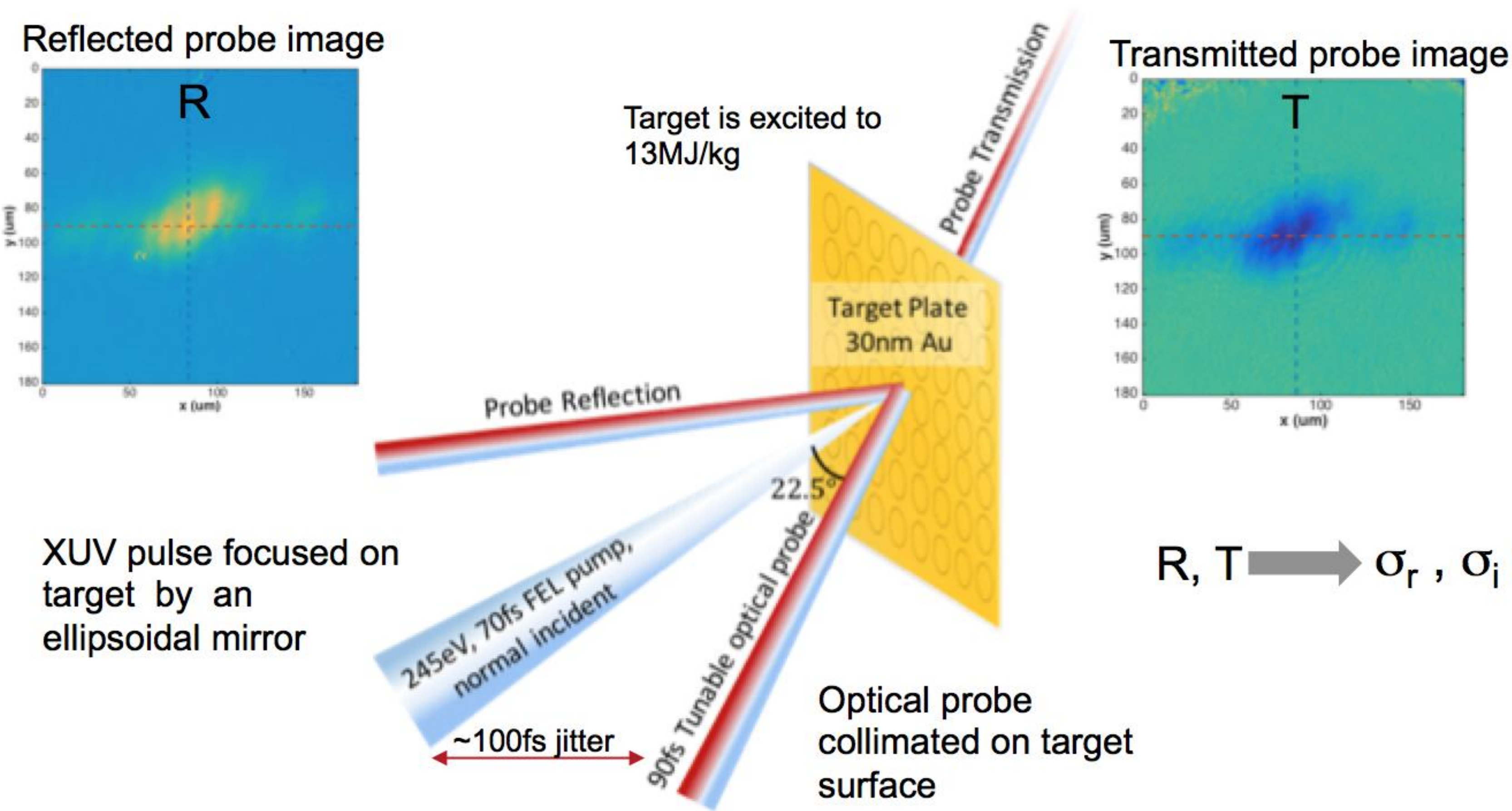

$$R, T \longrightarrow \sigma_r\ ,\ \sigma_i\ (\text{or}\ \varepsilon_r\ ,\ \varepsilon_i)$$

XUV Generated Warm Dense Gold

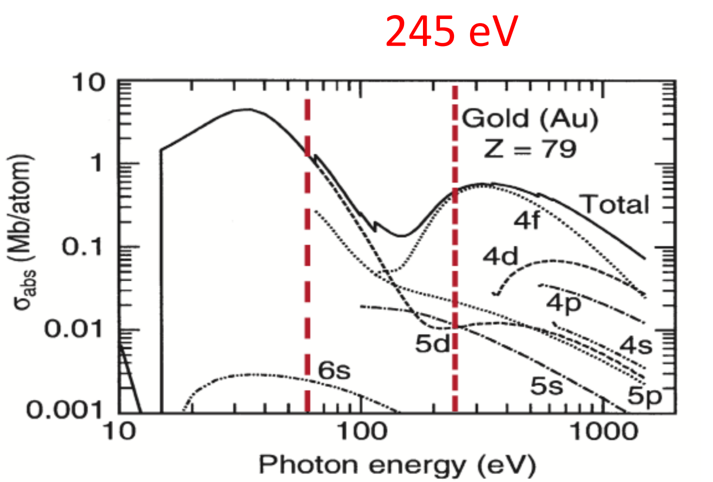

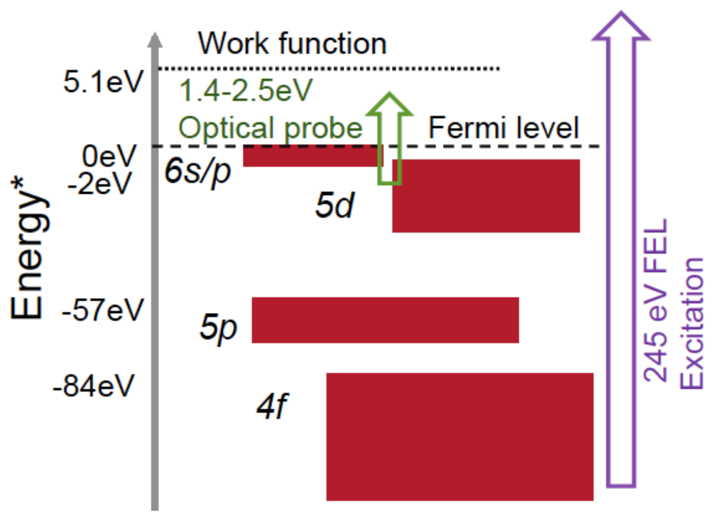

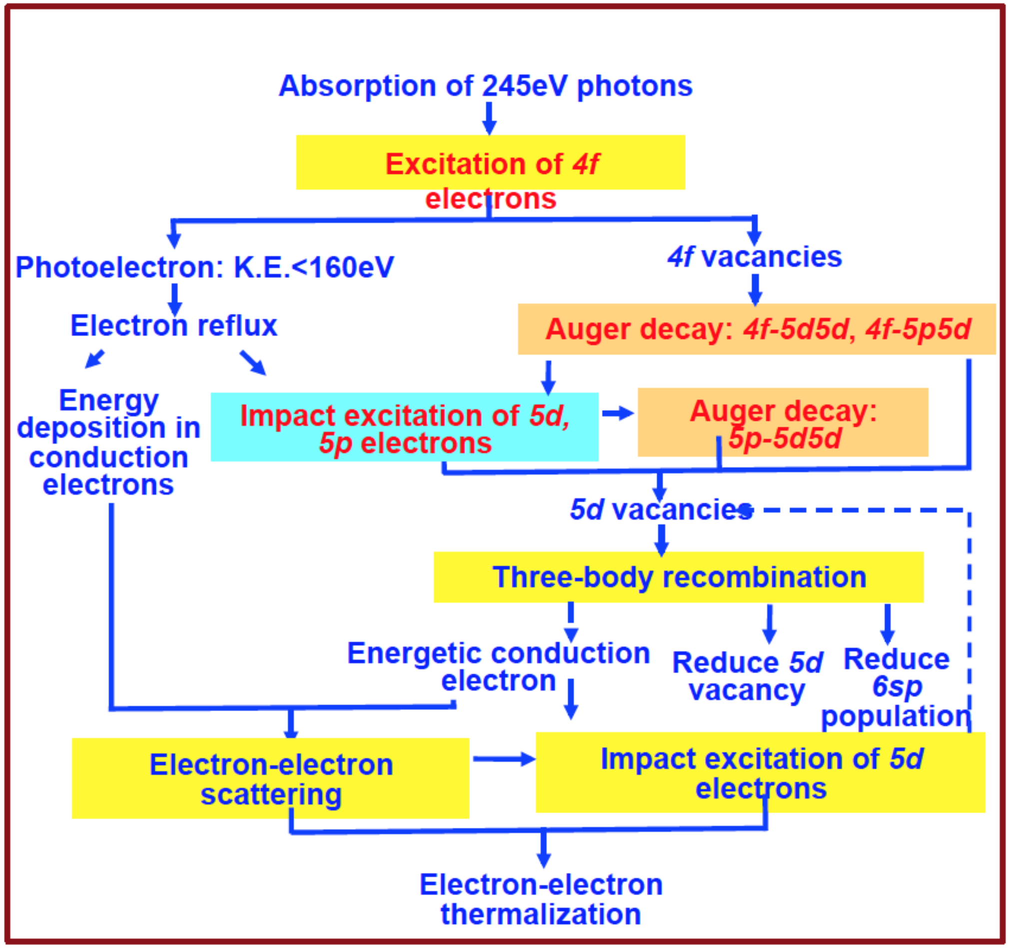

*Extracted from electron binding energy measurement by XPS (S. Thiess *et al*, Sol. State Commun. 132, 589 (2004)).

XUV versus Optical Generated Warm Dense Gold

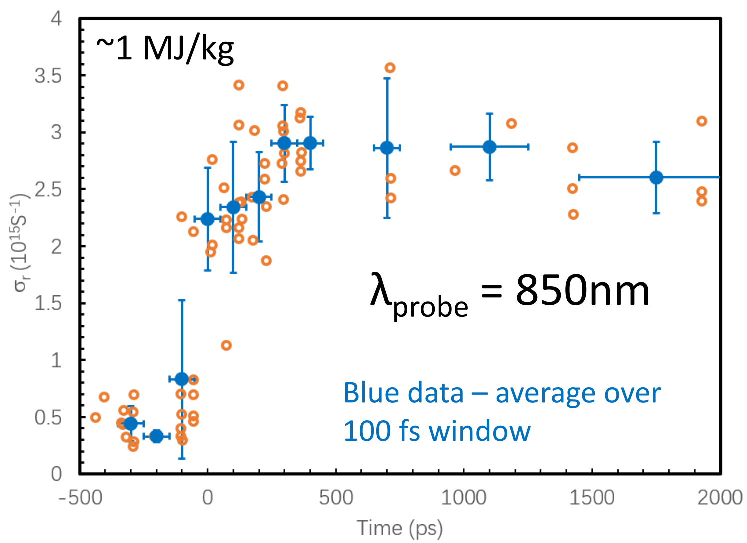

Non-thermalized WDM

- Response of FEL
  - ✧ 245eV photons can drive the electron system much further from equilibrium
  - ✧ Dependence on probe wavelengths and pump energy densities
  - ✧ Collaborating with theoretical groups (Ziaja – DESY, Recoule – CEA, Rethfeld – TU Kaiserslautern, Gericke – U Warwick) to gain better understanding of this uncharted regime

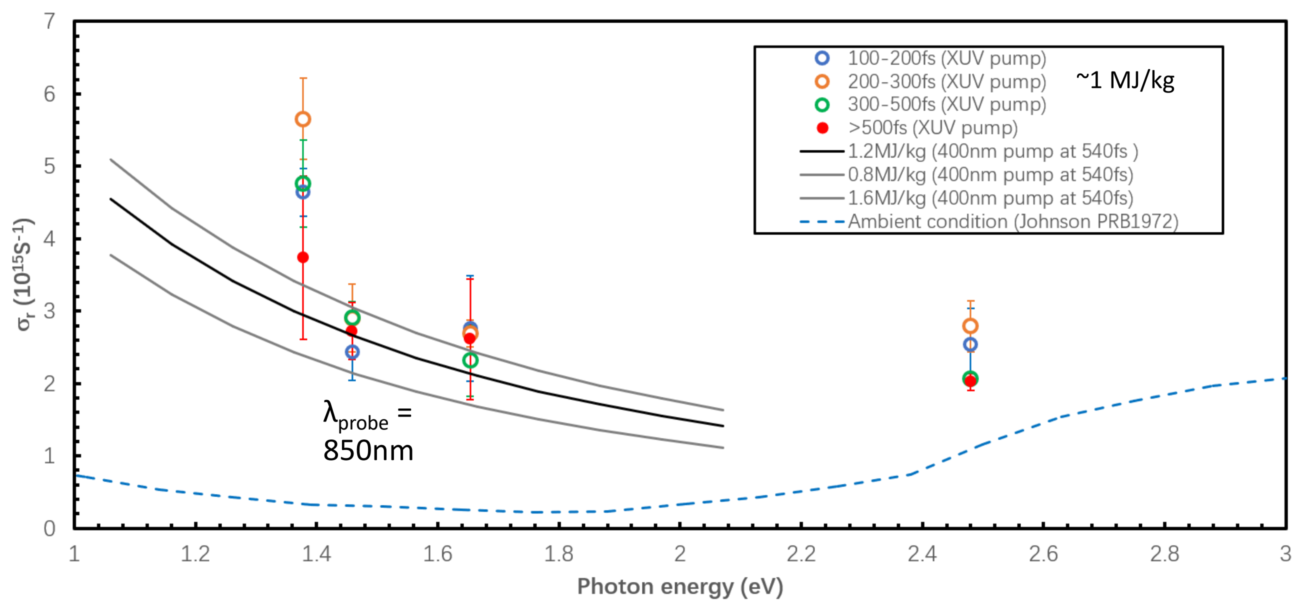

2T WDM

- Reasonable agreement between XUV and optical data at λ_{probe}= 850nm & 750nm but more differences at λ_{probe}= 900nm
- Differences in AC conductivity may reflect differences in electronic structure

Impacts

Knowledge gained are important for

- Better understanding the physics of ultrafast laser materials interaction and optimizing applications
- Warm Dense Matter Theories development
- Fusion Energy
  - Inertial Confinement Fusion
  - Materials for Fusion Energy Reactors
- Planetary Science

Applications of Ultrafast Laser Materials Interaction

Frequency tuning of Si photonic devices fs-LMP

- Bachman etal, OE 21, 11048 (2013)

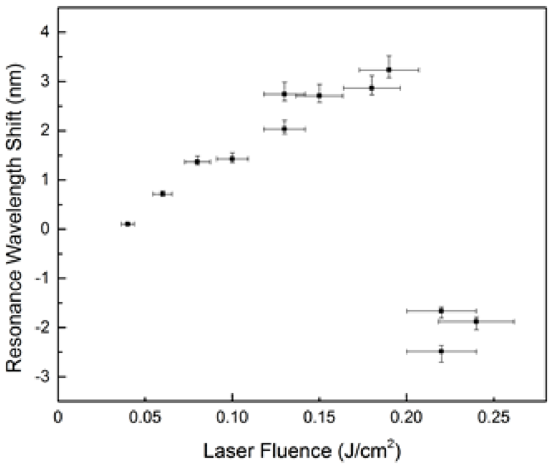

Si Microring Resonator

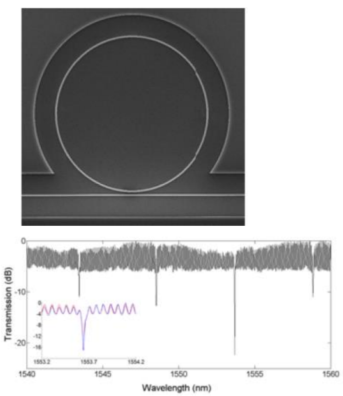

Transfer of sub-100 nm Cr dots using fs-LIFT

- Sametugo etal, OE 21, 18525 (2013)

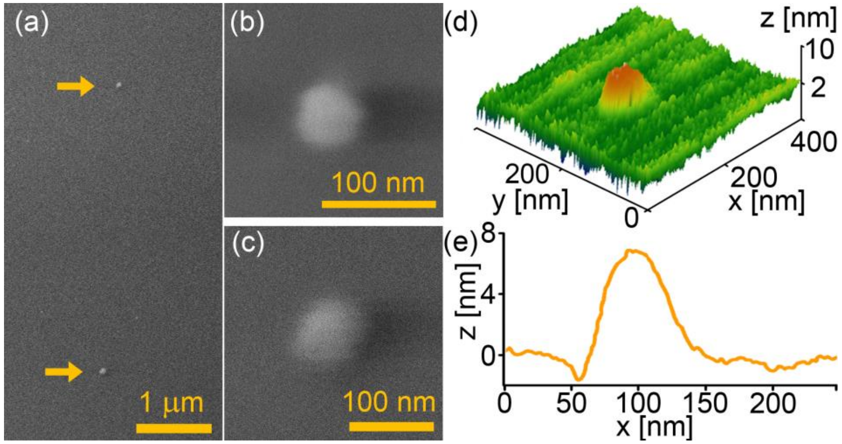

Mapping of fingerprints using fs-LIBS

- Taschuk etal, AS 60, 1322 (2006)

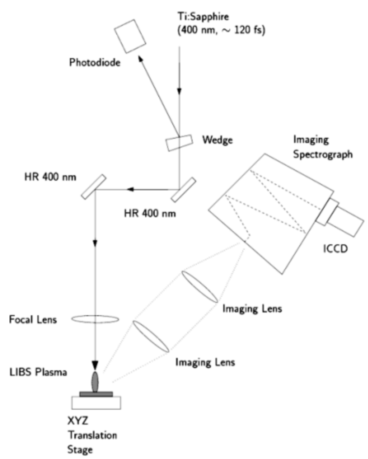

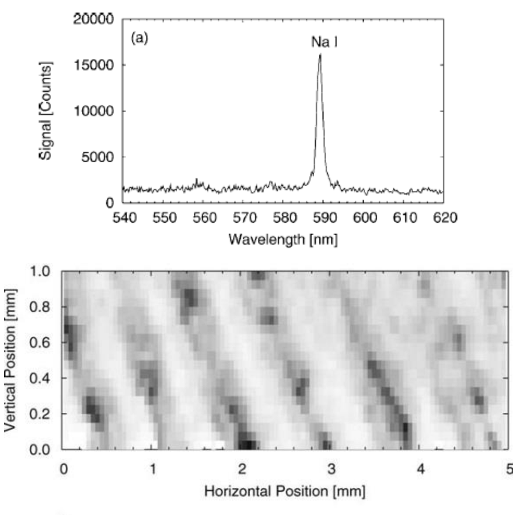

Crystalline nanoparticles generation using fs-PLD

- Reenaasa etal, ASS 354, 206 (2015)

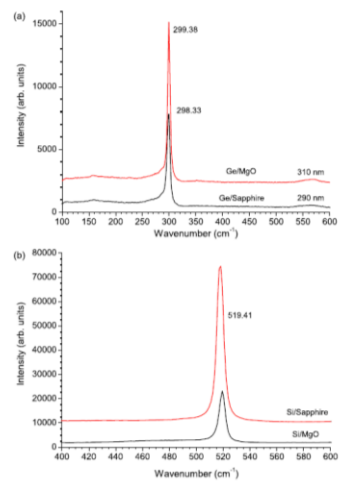

Fig. 8. Raman spectra of fs laser deposited (a) Ge and (b) Si films.

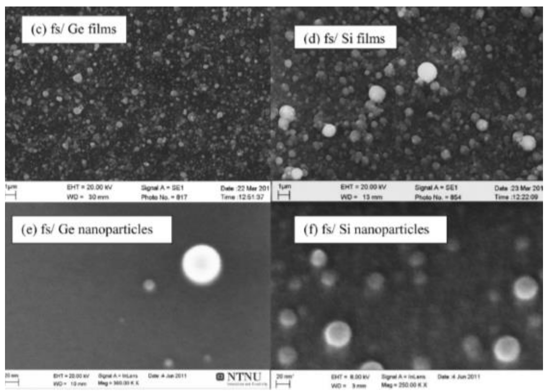

Inertial Confinement Fusion

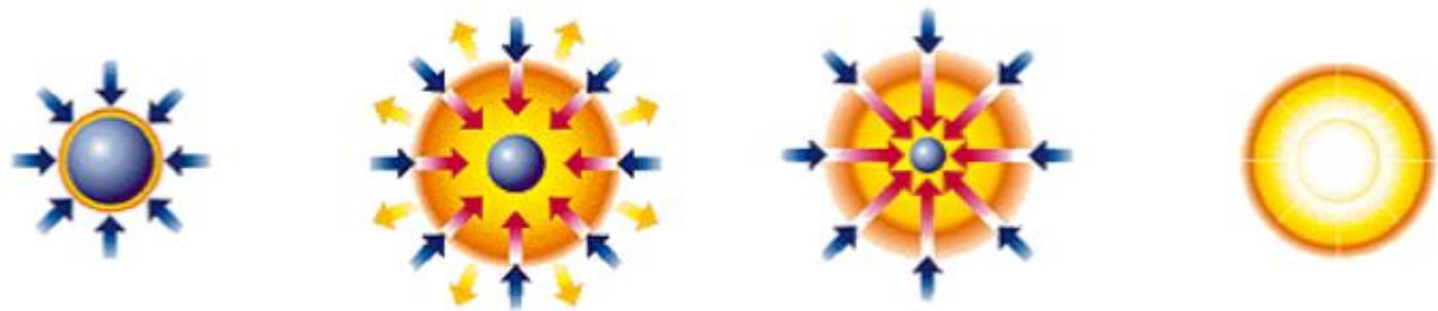

1) Atmosphere formation: Laser beams rapidly heat the surface of the fusion target forming a surrounding plasma envelope.

2) Compression: Fuel is compressed by the rocket-like blowoff of the hot surface material.

3) Ignition: During the final part of the laser pulse, the fuel core reaches 20 times the density of lead and ignites at 100,000,000 degrees Celsius.

4) Burn: Thermonuclear burn spreads rapidly through the compressed fuel, yielding many times the input energy.

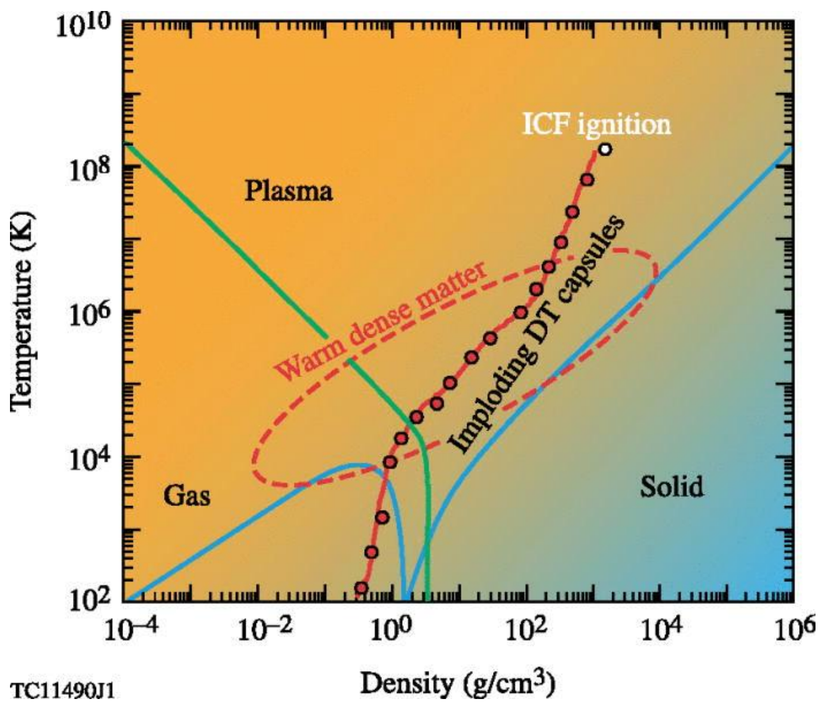

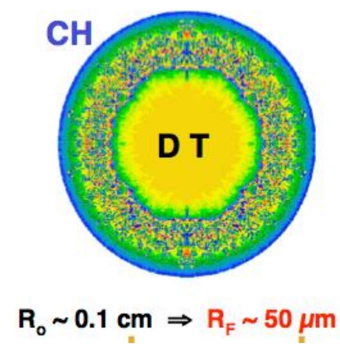

In ICF, the fuel capsule containing ^{2}H Deuterium & ^{3}H Tritium will go through various states including condensed matter, **warm dense matter** and plasma

Fusion Energy Reactors

Detailed understanding of damage mechanisms for materials under extreme conditions is important for designing fusion reactor materials

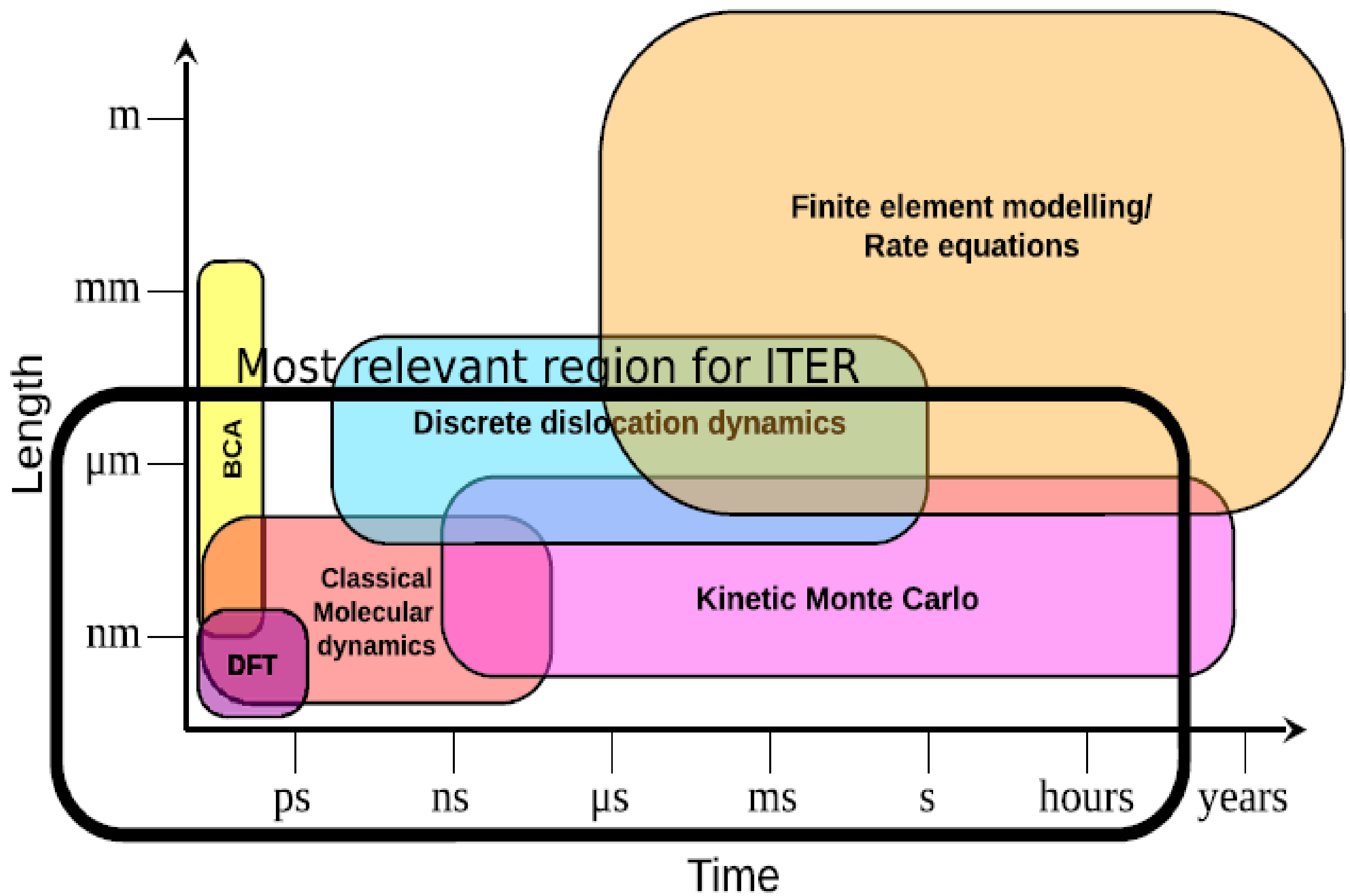

Planetary Science

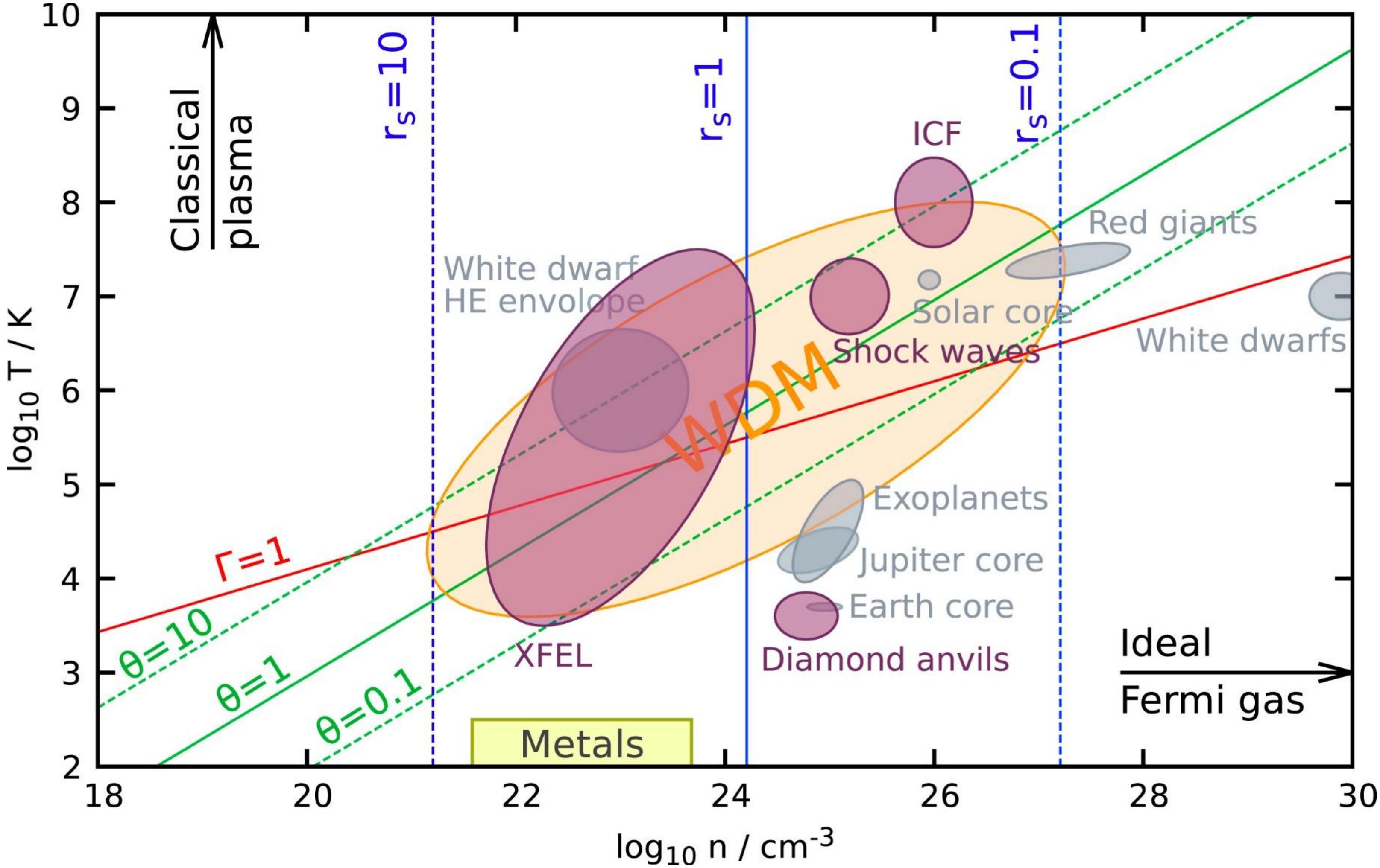

Dornheim, Physics Reports 744, 1 (2018)

Summary

- Two temperature Warm Dense Gold produced by 400nm 45fs laser pulse on 30nm thick free standing gold foil is studied by ultrafast optical and MeV electron probes
- Agreement in experimental and calculated σ_{AC}(t≈0.5ps) **corroborating DFT calculations of C_{ei}**
- Both optical and UED experimental data pointed to **g_{ei} with weak temperature dependency**

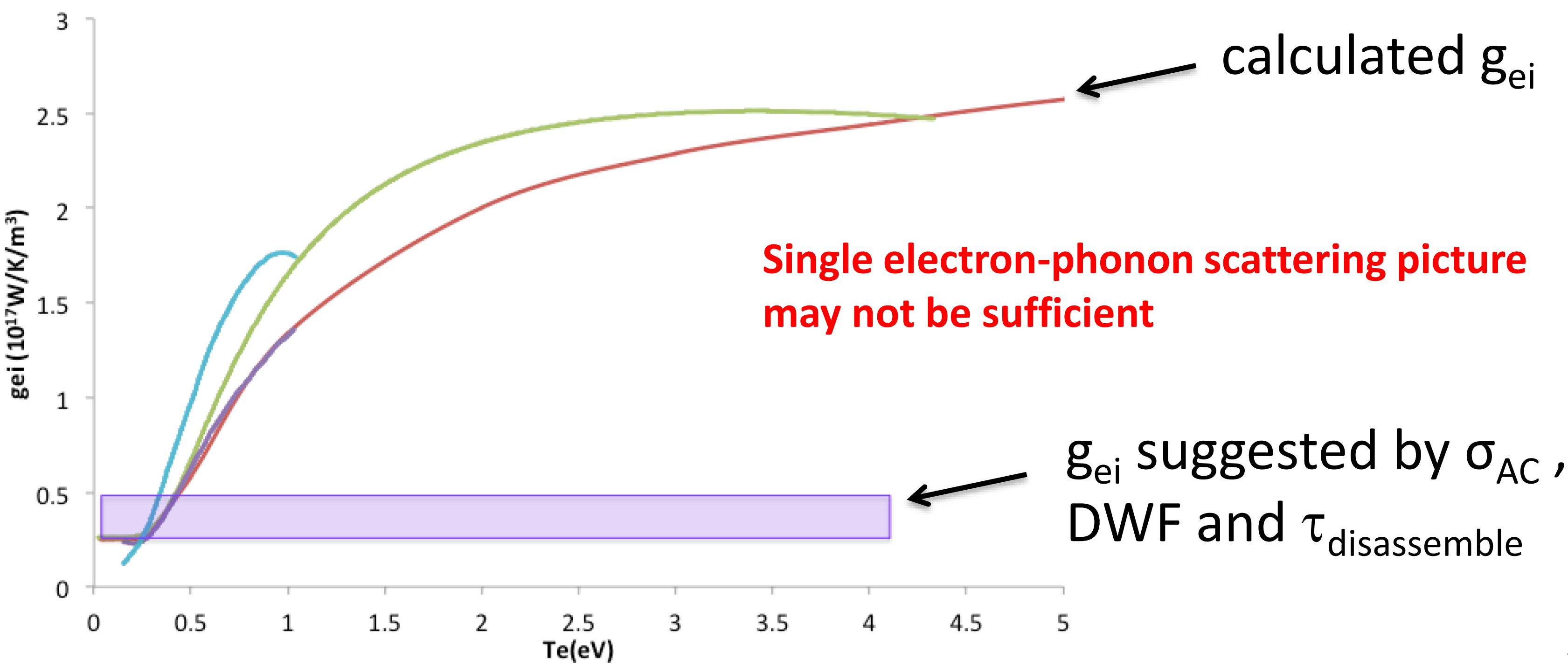

Summary

- Homogenous melting and heterogeneous melting

homogenous melting

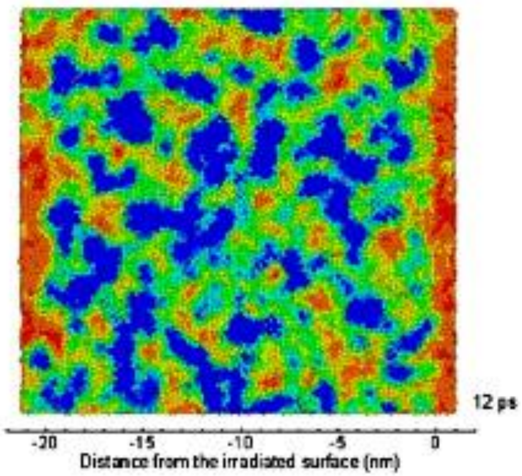

heterogeneous melting (**first observation**)

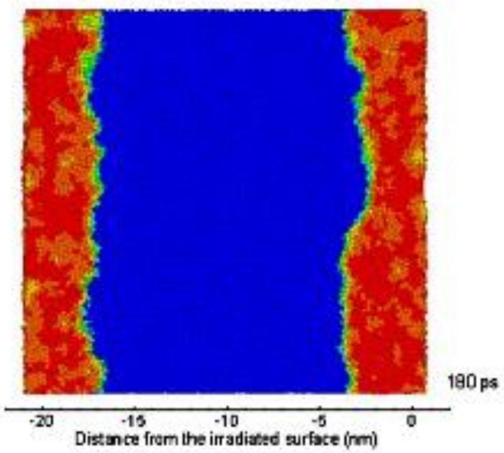

- XUV versus Optical
  Non-thermalized WDM (**uncharted**)
  - XUV can drive the electron system much further from equilibrium
  2T WDM
  - Differences in AC conductivity may reflect differences in electronic structure

- WDM is important for
  - Ultrafast laser materials interactions
  - Fusion energy
  - Planetary science

Acknowledgement

Y. Y. Tsui
Z. Chen
V. Sametoglu
S. E. Kirkwood
M. Reid
B. Russell
C. Curry
R. Zhang

A. Ng

S. H. Glenzer
Z. Chen
P. Hering
M. Mo
B. Russell
C. Curry
& others

V. Recoules
L. Soulard
B. Holst

S. Toleikis
B. Ziajia
& others